Quantum Chemical Cluster Modeling of Enzymatic Reactions

Rong-Zhen Liao

ISBN 978-91-7447-129-8

Printed in Sweden by US-AB, Stockholm 2010

Distributor: Department of Organic Chemistry, Stockholm University

Abstract

The Quantum chemical cluster approach has been shown to be quite powerful and efficient in the modeling of enzyme active sites and reaction mechanisms. In this thesis, the reaction mechanisms of several enzymes have been investigated using the hybrid density functional B3LYP. The enzymes studied include four dinuclear zinc enzymes, namely dihydroorotase, N-acyl-homoserine lactone hydrolase, RNase Z, and human renal dipeptidase, two trinuclear zinc enzymes, namely phospholipase C and nuclease P1, two tungstoenzymes, namely formaldehyde ferredoxin oxidoreductase and acetylene hydratase, aspartate α-decarboxylase, and mycolic acid cyclopropane synthase. The potential energy profiles for various mechanistic scenarios have been calculated and analyzed. The role of the metal ions as well as important active site residues has been discussed.

In the cluster approach, the effects of the parts of the enzyme that are not explicitly included in the model are taken into account using implicit solvation methods. With aspartate α-decarboxylase as an example, systematic evaluation of the solvation effects with the increase of the model size has been performed. At a model size of 150-200 atoms, the solvation effects almost vanish and the choice of the dielectric constant becomes rather insignificant.

For all six zinc-dependent enzymes studied, the di-zinc bridging hydroxide has been shown to be capable of performing nucleophilic attack on the substrate. In addition, one, two, or even all three zinc ions participate in the stabilization of the negative charge in the transition states and intermediates, thereby lowering the barriers. In dihydroorotase and human renal dipeptidase, the protonation states of an important active site carboxylate residue, being ionized or neutral, have been considered. In N-acyl-homoserine lactone hydrolase, two different substrate orientations have been taken into account. In phospholipase C, two different mechanisms with either a bridging hydroxide or a terminal water molecule as the nucleophile have been

analyzed. In nuclease P1, the reactions of both phosphate monoester and diester substrates have been explored.

For the two tungstoenzymes, several different mechanistic scenarios have been considered to identify the energetically most feasible one. For both enzymes, new mechanisms are proposed. In formaldehyde ferredoxin oxidoreductase, a proton transfer coupled with a two-electron transfer to W^{VI} has been found to be crucial for the intermediate oxidation. In acetylene hydratase, W^{IV} has been suggested to activate the acetylene substrate for a nucleophilic attack and stabilize the carboanion transition states and intermediates.

Finally, the mechanism of mycolic acid cyclopropane synthase has been shown to be a direct methyl transfer to the substrate double bond, followed by proton transfer to the bicarbonate.

From the studies of these enzymes, we demonstrate that density functional calculations are able to solve mechanistic problems related to enzymatic reactions, and a wealth of new insight can be obtained.

List of papers included in this thesis

I. Theoretical Investigation of the Reaction Mechanism of the Dinuclear Zinc Enzyme Dihydroorotase.

Liao, R.-Z.; Yu, J.-G.; Raushel, F. M.; Himo, F.

Chem. Eur. J. **2008**, 14, 4287-4292.

II. Reaction Mechanism of the Dinuclear Zinc Enzyme N-acyl-L-homoserine Lactone Hydrolase: a Quantum Chemical Study.

Liao, R.-Z.; Yu, J.-G.; Himo, F.

Inorg. Chem. **2009**, 48, 1442-1448.

III. Theoretical Study of the RNA Hydrolysis Mechanism of the Dinuclear Zinc Enzyme RNase Z

Liao, R.-Z.; Himo, F.; Yu, J.-G.; Liu, R.-Z.

Eur. J. Inorg. Chem. **2009**, 20, 2967-2972.

IV. Dipeptide Hydrolysis by the Dinuclear Zinc Enzyme Human Renal Dipeptidase: Mechanistic Insights from DFT Calculations

Liao, R.-Z.; Himo, F.; Yu, J.-G.; Liu, R.-Z.

J. Inorg. Biochem. **2010**, 104, 37-46.

V. Reaction Mechanism of the Trinuclear Zinc Enzyme Phospholipase C – A Density Functional Theory Study

Liao, R.-Z.; Yu, J.-G.; Himo, F.

J. Phys. Chem. B **2010**, 114, 2533-2540.

VI. Phosphate Mono- and Diesterase Activities of the Trinuclear Zinc Enzyme Nuclease P1— Insights from Quantum Chemical Calculations

Liao, R.-Z.; Yu, J.-G.; Himo, F.

Inorg. Chem. **2010**, 49, 6883-6888.

VII. Quantum Chemical Modeling of Enzymatic Reactions: The Case of Decarboxylation

Liao, R.-Z.; Yu, J.-G.; Himo, F.

Manuscript.

VIII. Tungsten-dependent Formaldehyde Ferredoxin Oxidoreductase — Reaction Mechanism from Quantum Chemical Cluster Calculations

Liao, R.-Z.; Yu, J.-G.; Himo, F.

Submitted for publication.

IX. Enzymatic Acetylene activation: Mechanism of Tungsten-dependent Acetylene hydratase from Quantum Chemical Calculations

Liao, R.-Z.; Yu, J.-G.; Himo, F.

Submitted for publication.

X. Mechanism of Mycolic Acid Cyclopropane Synthase: A Theoretical Study

Liao, R.-Z.; Yu, J.-G.; Himo, F.

Submitted for publication.

Reprints were made with kind permission from the publishers.

Comments on my contributions to the papers

I was responsible for all calculations and the preparation of all manuscripts.

List of papers not included in this thesis

XI. Water Assisted Transamination of Glycine and Formaldehyde

Liao, R.-Z.; Ding, W.-J.; Yu, J.-G.; Fang, W.-H.; Liu, R.-Z.

J. Phys. Chem. A **2007**, 111, 3184-3190.

XII. Highly Efficient and Site-selective [3+2] Cycloaddition of Carbene-derived Ambient Dipoles with Ketenes for a Straightforward Synthesis of Spiro-pyrrolidones

Li, J.-Q.; **Liao, R.-Z.**; Ding, W.-J.; Cheng, Y.

J. Org. Chem. **2007**, 72, 6266-6269.

XIII. Theoretical Studies on Pyridoxal 5'-Phosphate-Dependent Transamination of a-Amino Acids

Liao, R.-Z.; Ding, W.-J.; Yu, J.-G.; Fang, W.-H.; Liu, R.-Z.

J. Comput. Chem. **2008**, 29, 1919-1929.

XIV. DFT Study on the Mechanism of *Escherichia coli* Inorganic Pyrophosphatase

Yang, L.; **Liao, R.-Z.**; Yu, J.-G.; Liu, R.-Z.

J. Phys. Chem. B **2009**, 113, 6505-6510.

XV. DFT study of the Asymmetric Nitroaldol (Henry) Reaction Catalyzed by a Dinuclear Zn Complex

Qi, N.; **Liao, R.-Z.**; Yu, J.-G.; Liu, R.-Z.

J. Comput. Chem. **2010**, 31, 1376-1384.

XVI. DFT Studies of the Degradation Mechanism of the Methyl-mercury Activated by Sulfur-rich Ligand

Li, X.-C.; **Liao, R.-Z.**; Zhou, W.-C.; Chen, G.-J.

Phys. Chem. Chem. Phys. **2010**, 12, 3961-3971.

Contents

Abbreviations

AH	Acetylene hydratase
AHL lactonase	N-acyl Homoserine Lactone hydrolase
AOR	Aldehyde Oxidoreductase
AspDC	$_{L}$-Aspartate α-decarboxylase
CFAS	Cyclopropane Fatty Acid Synthase
CPCM	Conductor-like Polarizable Continuum Model
DFT	Density Functional Theory
DHO	Dihydroorotase
FOR	Formaldehyde Ferredoxin Oxidoreductase
GGA	Generalized Gradient Approximation
HF	Hartree-Fock
hrDP	Human Renal Dipeptidase
LDA	Local Density Approximation
MACS	Mycolic Acid Cyclopropane Synthase
MFJ	More O'Ferrall Jencks
MUE	Mean Unsigned Error
NP1	Nuclease P1
PDB	Protein Data Bank
PES	Potential Energy Surface
PLC	Phospholipase C
QM/MM	Quantum Mechanics and Molecular Mechanics
TS	Transition State
TST	Transition State Theory
ZPE	Zero-Point Energy

Amino acid abbreviations

A/Ala	Alanine
C/Cys	Cysteine
D/Asp	Aspartate
E/Glu	Glutamate
F/Phe	Phenylalanine
G/Gly	Glycine
H/His	Histidine
I/Ile	Isoleucine
K/Lys	Lysine
L/Leu	Leucine
M/Met	Methionine
N/Asn	Asparagine
P/Pro	Proline
Q/Gln	Glutamine
R/Arg	Arginine
S/Ser	Serine
T/Thr	Threonine
V/Val	Valine
W/Trp	Tryptophan
Y/Tyr	Tyrosine

Chapter 1

Introduction

A Catalyst is a substance that changes the reaction rate without being consumed itself. It reacts with substrates affording intermediates if necessary, and subsequently harvests products with the regeneration of itself. Since the catalyst is regenerated during the reaction, generally only a small amount is needed for the rate enhancement. Catalysts are usually divided into homogeneous catalysts, heterogeneous catalysts, and biocatalysts. Enzymes are important biocatalysts that mediate most chemical transformations in organisms under mild conditions, and are involved in cell growth, food metabolism, signaling, regulation, and energy transduction. Enzymes are composed of tens of thousands of atoms, but the catalytic reaction occurs in a small region called the active site. Many enzymes need cofactors for their activity, which can be organic molecules or metal ions, like Mg^{2+}, Ca^{2+}, Mn^{2+}, Fe^{2+}, Cu^{2+}, Zn^{2+} , Mo^{4+}(or Mo^{6+}) and W^{4+} (or W^{6+}).

Zn^{2+} has an electronic configuration of $3d^{10}$ and no redox property in biology. It can play both structural and catalytic roles in enzymes. In addition, it can be reversibly coordinated to both soft and hard (N, O, S) ligands, like Asp, Glu, His, Cys, water, with rather flexible coordination numbers (4 to 6) and structures, without dependence on ligand-field stabilization. Furthermore, Zn is the second most abundant heavy metal, existing in all six classes of enzymes, oxidoreductases, transferases, hydrolases, lyases, isomerizases, and ligases. In hydrolases, zinc enzymes catalyze the hydrolysis of peptides, amides, carboxylic esters, phosphate, sulfates, etc. A water molecule or a hydroxide is believed to coordinate to the zinc ion, functioning as a nucleophile or a base for the reaction. In the active site, there can be one, two or even three zinc ions. For dinuclear zinc enzymes, the zinc centers are often bridged by an oxygen species and an aspartate residue. The removal of one or more zinc ions results in dramatic decrease of catalytic activity or even inactivation. Considerable efforts have been devoted to the understanding of why some enzymes choose two or even three zinc ions for their activity. It has been proposed that two (or three) zinc ions can independently play either a catalytic or a structural role, and they can catalyze different chemical steps in multistep reactions. In addition, the two (or three) zinc ions can activate substrates through binding with more than one atom of polyatomic substrates, like phosphates and sulfates, which may bind the two (or three) metal ions through two of their oxygens. Furthermore, the two zinc ions

together can easily lower the pK_a of the bridging water molecule, forming the nucleophilic hydroxide.

Tungsten is the heaviest chemical element in biology and its oxidation state varies from +4 to +6 in tungstoenzymes. It is involved in the enzymatic hydration of acetylene (acetylene hydratase), and oxidation of aldehyde (aldehyde oxidoreductases) and formate (formate dehydrogenases), offering an energy source for some bacteria. In the active site, the tungsten ion is seen to be bound to two pterin cofactors. For aldehyde oxidoreductases, a W^{VI}=O is suggested to be utilized for substrate oxidation. For acetylene hydratase, W^{4+} is believed to be the reactive species. The role of tungsten in enzymes is still not clear.

Quantum chemical methods have become a very powerful approach in modeling enzymes and catalytic mechanisms. Profound mechanistic insights can be acquired through reaction pathway investigations. With the development of density functional theory methods, especially the hybrid functional B3LYP, the cluster methodology for modeling enzyme active site has been successfully utilized to the studies of a large number of enzymes. Nowadays, it is quite robust to handle chemical systems with 100 to 200 atoms at reasonable levels of accuracy and speed. A model of the active site can be designed from the X-ray crystal structure. For metalloenzymes, the active site models usually contain the metal ions and their first-shell ligands, together with some important second-shell residues and model of substrate. The protein surrounding is approximately treated as a homogeneous continuum model with some dielectric constant. This protocol has been found to be every efficient in reaction pathway calculations, in which geometric changes can be traced and the role of various parts can be deduced. Understanding how enzymes catalyze and control their reactions is of fundamental importance and can have many practical implications, for example, design of inhibitors and new medicines, synthesis of biomimetic complexes, applications of bio-transformations in industrial processes.

In this thesis, density functional theory is applied to investigate the reaction mechanisms of six zinc enzymes, dihydroorotase (DHO), N-acyl homoserine lactone hydrolase (AHL lactonase), RNase Z, human renal dipeptidase (hrDP), phospholipase C (PLC), and Nuclease P1 (NP1), two tungstoenzymes, formaldehyde ferredoxin oxidoreductase and acetylene hydratase, as well as mycolic acid cyclopropane synthase. The modeling strategies and methodologies are able to explain experimental findings and rationalize factors governing the catalysis.

The thesis is organized in the following way. First, a brief outline of density functional theory is given in **Chapter 2**, followed by a short description of the methodology used for

modeling enzymes (**Chapter 3**). The results concerning dinuclear and trinuclear zinc enzymes are discussed in **Chapters 4** and **5**, respectively. The mechanisms of two tungstoenzymes are presented in **Chapter 6** and the mycolic acid cyclopropane synthase in **Chapter 7**. Finally, some general mechanistic features and conclusions for these enzymes are summarized in **Chapter 8**.

Chapter 2

Density functional theory

Molecular properties, like, for example, geometries, energies, and frequencies, can be calculated mathematically based on traditional quantum chemical methods, ranging from semi-empirical to advanced post Hartree-Fock. In these methods, an electronic wavefunction is used as the basic variable, depending on 4N coordinates (3N spatial and N spin) for an N-electron system. However, good accuracy can only be achieved for relatively small systems. To handle much larger systems (up to 100 atoms or more), an alternative approach has been developed, namely density functional theory (DFT). In DFT, the electron density function $\rho(r)$, depending on only 3 spatial coordinates, is used to calculate the properties of the system. In this thesis, mainly the hybrid DFT functional B3LYP is used in most calculations. A brief discussion of DFT and B3LYP will be presented in this chapter. A more comprehensive description of traditional quantum chemical methods and DFT is available in standard textbooks.[1-7]

2.1 Hohenberg-Kohn theorems

Employing electron density rather than wavefunction appears to be more promising due to its much less coordinate dependence as mentioned above. However, it was not proven that there exists a unique relationship between $\rho(r)$ and all fundamental properties of a given system, until the publication of the landmark paper by Hohenberg and Kohn in 1964.[8]

Within the Born-Oppenheimer approximation, the electronic Schrödinger equation is written as below:

$$\hat{H}_{elec}\psi_{elec}(r_i, R_A) = \varepsilon_{elec}\psi_{elec}(r_i, R_A) \qquad (2\text{-}1)$$

$$\text{Where } \hat{H}_{elec} = -\sum_{i=1}^{N}\frac{1}{2}\nabla_i^2 - \sum_{i=1}^{N}\sum_{A=1}^{M}\frac{Z_A}{r_{iA}} + \sum_{i=1}^{N}\sum_{j>i}^{N}\frac{1}{r_{ij}} \qquad (2\text{-}2)$$

In the Hamiltonian operator, since the second term (external potential $v(r)$) is the only one that is system-dependent, if $v(r)$ is known, then both $\hat{H}$ and Ψ are determined, and $\rho(r)$ can be obtained as:

$$\rho(r) = N\int\cdots\int\left|\Psi(x_1, x_2, \cdots x_N)\right|^2 d\sigma_1 dx_2 \cdots dx_N \qquad (2\text{-}3)$$

Thus $\rho(r)$ is a functional of $\nu(r)$ and Ψ. Hohenberg and Kohn[8] proved that $\nu(r)$ and Ψ are unique functionals of $\rho(r)$ (the first theorem) by *reductio ad absurdum*. It is impossible that two external potentials, differing by more than one additive constant, give the same ground state electron density. In other words, the external potential $\nu(r)$ is a unique potential of $\rho(r)$. Therefore, the ground state electron density $\rho_0(r)$ determines all ground state properties, like N, $\nu(r)$, Ψ_0 and E_0. The ground state electronic energy can be expressed as:

$$E[\rho]=V_{ne}[\rho]+T[\rho]+V_{ee}[\rho] \quad (2\text{-}4)$$

Where V_{ne}, T, V_{ee} are terms from nuclear potential, kinetic energy, and electron-electron interactions, respectively.

The second theorem provides the energy variational principle. It implies that for any trial electron density function $\rho(r)$, such that $\rho(r) \geq 0$ and $\int \rho(r)dr = N$,

$$E_0 \leq E[\rho(r)] \quad (2\text{-}5)$$

Where E_0 is the true ground state energy.

These two theorems provide the theoretical foundation of using $\rho(r)$ rather than Ψ to calculate all ground state properties. However, they do not offer a practical way of determining the mathematical form of the universal functional.

2.2 Kohn-Sham approach

In 1965, Kohn and Sham[9] suggested an approach to the unknown universal functional by introducing the concept of a non-interacting reference system built from a set of one-electron orbitals, called Kohn-Sham orbitals (ϕ_i^{KS}). In this approach, the kinetic energy term (T) is divided into two parts, the kinetic energy (T_S) of a non-interacting reference system (with the same density as the real system), and a small correction term T_C due to electron-electron interaction:

$$T[\rho]= T_S[\rho]+ T_C[\rho] \quad (2\text{-}6)$$

The electron-electron repulsion term (V_{ee}) can also be separated into two parts: the classical charge-cloud coulomb repulsion (J) and a non-classical electron-electron repulsion (E_{ncl}), containing exchange and correlation.

$$V_{ee}[\rho]=J[\rho]+E_{ncl}[\rho] \quad (2\text{-}7)$$

$$\text{Where } J[\rho]= \frac{1}{2}\iint \frac{\rho(r_1)\rho(r_2)}{r_{12}}dr_1dr_2 \quad (2\text{-}8)$$

In the Kohn-Sham scheme, the two unknown terms ($T_C[\rho]$and $E_{ncl}[\rho]$) are incorporated as

exchange-correlation functional $E_{xc}[\rho]$, which is divided into two parts, exchange $E_x[\rho]$ and correlation $E_c[\rho]$:

$$E_{xc}[\rho]= E_x[\rho]+ E_c[\rho] \tag{2-9}$$

The energy can be expressed as:

$$\begin{aligned} E[\rho(r)] &= T_S[\rho(r)] + J[\rho(r)] + E_{XC}[\rho(r)] + E_{Ne}[\rho(r)] \\ &= T_S[\rho(r)] + \frac{1}{2}\iint \frac{\rho(r_1)\rho(r_2)}{r_{12}} dr_1 dr_2 + E_{XC}[\rho(r)] + \int V_{Ne}\rho(r) dr \\ &= -\frac{1}{2}\sum_i^N \left\langle \varphi_i^{KS} \middle| \nabla^2 \middle| \varphi_i^{KS} \right\rangle + \frac{1}{2}\sum_i^N \sum_j^N \iint \left|\varphi_i^{KS}(r_1)\right|^2 \frac{1}{r_{12}} \left|\varphi_i^{KS}(r_2)\right|^2 dr_1 dr_2 \\ &+ E_{XC}[\rho(r)] - \sum_i^N \int \sum_A^M \frac{Z_A}{r_{1A}} \left|\varphi_i^{KS}(r_1)\right|^2 dr_1 \end{aligned} \tag{2-10}$$

Constructing a Slater determinant from ϕ_i^{KS} and minimizing the total energy under the normalization constraint of $\left\langle \phi_i^{KS} \middle| \phi_j^{KS} \right\rangle = \delta_{ij}$ leads to the Kohn-Sham equations:

$$\left(-\frac{1}{2}\nabla^2 + V_{eff}(r_1) \right) \phi_i^{KS} = \varepsilon_i \phi_i^{KS} \tag{2-11}$$

Where $V_{eff}(r) = \int \frac{\rho(r_2)}{r_{12}} dr_2 + V_{XC}(r_1) - \sum_A^M \frac{Z_A}{r_{1A}}$ and $V_{XC} = \frac{\delta E_{XC}}{\delta \rho}$

$V_{eff}(r)$ is electron density-dependent, and thus equation (2-11) has to be solved iteratively. If the exact mathematical form of the V_{XC} (potential due to the exchange-correlation energy E_{XC}) were known, this equation would yield the exact energy and electron density. The Kohn-Sham method is in principle exact, and approximations come from the quest of exchange-correlation functional. There is no systematic strategy to improve approximate functionals. The inherent accuracy of a DFT method thus depends on the quality of the chosen exchange-correlation functional.

The local density approximation (LDA) assumes that the exchange-correlation energy at any point is a function of only the electron density at that point.[10-12] This approximation is suitable for systems with slowly varying densities, but overestimates binding energies and thus it is not good enough to be used to study chemical reactions. Real systems always have a spatial varying density, and generalized gradient approximation (GGA) treats this by introducing the dependence on the gradient of the density.[13-16] More recently, higher order density gradient is considered, which is termed meta-GGA.[17,18] In 1993, Becke suggested a hybrid method, which mixes a fractional of the exact exchange from Hartree-Fock picture and introduces three empirical parameters. This functional, called B3LYP[19,20] is usually

expressed as:

$$E_{xc}^{B3LYP} = (1-a)E_x^{Slater} + aE_x^{HF} + bE_x^{B88} + (1-c)E_c^{VWN} + cE_c^{LYP} \quad (2\text{-}12)$$

Where E_x^{Slater} is the Dirac-Slater exchange corresponding to the uniform electron gas, E_x^{HF} is the Hartree-Fock exchange, E_x^{B88} is the gradient correction to exchange,[14] E_c^{VWN} and E_c^{LYP} are the correlation functionals of Vosko, Wilkand Nusair[12] and Lee, Yang, and Parr[16], respectively. The three parameters a, b, c are 0.20, 0.72, and 0.81, respectively.

2.3 Performance of B3LYP

In this thesis, the most popular hybrid functional B3LYP is used to investigate the reaction mechanisms. Various assessments have been reported in the literature regarding the accuracy of B3LYP with respect to geometries and energies, which are the two crucial properties for the study of reaction mechanisms.

2.3.1. Accuracy on geometries

B3LYP usually performs very well in the prediction of geometrical parameters. Within the G2 set (55 small molecules, 71 bond lengths, 26 bond angles, and 2 dihedral angles), the average errors at the B3LYP/6-311+G(3*df*,2*p*) level of theory are 0.008 Å for bond lengths, 0.61° for bond angles, and, 3.66° for dihedral angles.[21]

Several assessments of B3LYP on the geometric parameters of zinc complexes, relevant for the enzymes studied in this thesis, have been made in recent years.

Sousa et al.[22] have accessed the accuracy of five density functionals and 15 different basis sets for 7 mononuclear zinc biological complexes. The mean unsigned error (MUE) in Zn-ligand bond distances is 0.09 Å at the B3LYP/6-311G(*d*,*p*) level. B3LYP was shown to have the best average performance in the test. They further compared 18 density functionals in the determination of 44 Zn-ligand bond distances and 60 ligand-Zn-ligand bond angles from 10 zinc complexes.[23] At the B3LYP/6-311G(*d*,*p*) level, the MUE in distances and angles are 0.071 Å, and 11.6°, respectively. With the 6-311G(*d*,*p*) basis sets, the BB1K and MPW1K functionals gave the lowest MUE in distances (0.063 Å), and G96LYP gave the lowest MUE in angles (8.1°).

Rayón et al.[24] have tested the performance of five density functionals in the prediction of Zn-Ligand distances (19 complexes) with a dataset obtained with the MP2 and CCSD(T) wavefunction methodologies. B3LYP gave a standard deviation of 0.019 Å with an aug-cc-

pVTZ basis sets.

Amin and Truhlar[25] have evaluated the performance of 39 density functionals in the determination of 10 Zn-Ligand bond distances (dataset obtained by CCSD(T) non-relativistic calculations). In this study, the best results were obtained with X3LYP (MUE=0.0069 Å), and B3LYP also rendered very good results (MUE=0.0080 Å). Recently, they also analyzed the performance of 4 density functionals (B3LYP, M05-2X, M06, and M06-2X) for 26 zinc containing species (dataset obtained with CCSD(T) method).[26] B3LYP gave the lowest MUE (0.025 Å) in Zn-ligand bond distances. The MUE of B3LYP for bond angles is 0.85°, quite close to that of M06-2X (MUE=0.60°).

These results show that B3LYP is accurate enough for geometry prediction, in particular for modeling of zinc-containing systems.

2.3.2. Accuracy on energies

The performance of B3LYP on energies, such as atomization energies, bond dissociation energies, and ionization energies, has also been evaluated. Within the G3/05 test set (454 energies with experimental uncertainties less than ±1 kcal/mol), the mean absolute deviation at the B3LYP/6-311+G(*3df,2p*)//MP2/6-31G(*d*) level (corrected by scaled (0.89) HF/6-31G(*d*) zero-point energies) is 4.1 kcal/mol.[27] Tirado-Rives and Jorgensen[28] have tested the performance of B3LYP for 622 neutral, closed-shell organic compounds containing C, N, O, and H. The mean absolute error in the heats of formation is 2.7 kcal/mol at the B3LYP/6-31+G(*d,p*) level.

Riley and Merz[29] have validated the performance of 12 density functionals in the heats of formation of 9 small zinc containing species and ionization potentials of 7 zinc compounds. For the heats of formation, BB1K (together with 6-31G(*d,p*) basis sets) gave the lowest MUE (8.8 kcal/mol), followed by B3LYP (MUE=8.9 kcal/mol). For the ionization potentials, B3LYP had the lowest MUE (1.03 eV).

Rayón et al.[24] have tested the performance of five density functionals in the prediction of binding energies of 19 Zn-Ligand complexes with a dataset obtained with the MP2 and CCSD(T) methods. With an aug-cc-pVTZ basis set, B3LYP gave a standard deviation of 2.79 kcal/mol for complexes with neutral ligands, and 3.27 kcal/mol with mono-anionic ligands.

Amin and Truhlar[25] have evaluated the performance of 39 density functionals in the determination of bond dissociation energies, considering a dataset of 12 Zn-Ligand complexes (obtained by coupled cluster nonrelativistic calculations). In this study, the best results were

obtained with M06-2X (MUE= 3.30 kcal/mol), while B3LYP also performed relatively well (MUE= 5.41 kcal/mol). They also assessed the performance of 4 density functionals (B3LYP, M05-2X, M06, and M06-2X) for 26 zinc containing species (dataset obtained with CCSD(T) method) with respect to bond dissociation energies. B3LYP gave a MUE of 6.04 kcal/mol.

The above data indicates that B3LYP performs well for reaction energies of zinc compounds. Currently, it is impossible to run extensive benchmark tests for enzymatic reactions since accurate experimental reference data is not available and high level *ab initio* calculations are prohibitive due to the large size of enzymes. Based on extensive modeling of a wide range of enzymes, Siegbahn concluded that B3LYP gives an error of less than 5 kcal/mol for enzyme modeling involving transition metals.[30]

2.4 Limitations of approximate density functionals

Despite the widespread popularity of DFT, approximate density functionals still have the potential to yield large errors in determining some properties. The three main formal deficiencies are self-interaction error, near-degeneracy error, and lack of description of dispersion. Yang and co-workers suggested that the failures of approximate density functionals can be traced to delocalization errors and static correlation errors.[31-34]

For a one-electron system, such as H_2^+, there is no electron-electron interaction, therefore the exchange energy must exactly cancel the Coulomb energy. However, most approximate functionals cannot properly account for this. When H_2^+ dissociates, the system converges to a delocalized state, with half electron located at each center ($H^{0.5+}$ + $H^{0.5+}$), rather than the correct localized state (H + H^+). This is because the delocalized state exhibits less self-interaction, which is repulsive. The error of bond dissociation energy for H_2^+ is as large as 55 kcal/mol at the B3LYP/6-311G(*d*,*p*) level. For many-electron systems, it is called delocalization error, reflecting the tendency to spread out the electron density artificially. The physical nature of this error has been related to the incorrect description of systems with fractional charges. In reality, the energy is a linear function of the fractional charges. Most approximate functionals yield an incorrect convex behavior. However, HF method gives an opposite concave behavior and thus suffers from localization error. For chemical reactions, the delocalization error tends to predict lower transition state energies because the transition state has electrons delocalized over more than one center. Therefore, most pure DFT methods predict lower barrier heights. However, hybrid functionals, like B3LYP, benefit from some error cancellation and have better performance in barrier height calculations.

A covalent bond is described well by approximate functionals, however, because of the sing-determinant nature of the Kohn-Sham orbitals, the bond dissociation energy is always overestimated. The exchange-correlation functional is inherently local, thus it is unsuitable for accounting the long range static correlation due to degeneracy or near degeneracy. A fraction-spin state has been used to analyze the interaction of degenerate states. In reality, the energy is a constant as a function of fractional spins. Both HF and approximate functionals give the wrong curve. In contrast to delocalization error, thus error tends to raise barrier heights. The B3LYP method used in this thesis appears in many cases balances these two errors quite well.

It should be noted that approximate functionals lack the description of van der Waals interaction. A tendency for exaggerated repulsion appears when atoms are forced to be close to each other in molecules. Due to this, π-stacking, like in DNA, cannot be accurately treated.[35] This could, for example, result in an underestimation of the binding energy of substrate into the enzyme active site.[36,37] To solve this problem, a empirical $-C_6/R^6$ term has been suggested to be added to account for long-range interaction.[38]

Chapter 3

Modeling approach of enzyme catalysis

Quantum chemical methods have in recent years been successfully adopted to analyze reaction pathways of enzymes at atomic levels. The available computer power can treat systems of more than 200 atoms with DFT method. However, this is still far from the size of enzymes, which usually contain thousands of atoms. The reactions are usually catalyzed at a rather small region of the enzyme, named active site, with several well-defined functional groups, like amino acids, cofactors, metal ions, water molecules, and so on. The catalytic effect of enzyme is thus to a large extent quite local at the active site, and the effects of the active site surrounding are usually of lower order. In the present thesis, a cluster approach is used for modeling enzyme active sites and reaction mechanisms. A relative small but well-chosen model of the active site, which is typically over 100 atoms, is considered and treated with DFT method. The polarization effects of the enzyme environment are handled by homogeneous continuum methods. The steric effects imposed by the protein matrix are taken into account by locking certain key atoms at the periphery of the active site model. This methodology has been found to be very useful and been successfully applied to a large number of enzymes.[39-51] Before the discussion of the enzymes investigated, a brief introduction to some concepts in enzyme catalysis and the idea of the cluster approach will be given in this chapter.

3.1 Enzyme catalysis

The proficiency of enzyme catalysis is defined as the ratio of the second-order rate constant of the enzymatic reaction (k_{cat}/K_M) and the rate constant of the same uncatalyzed reaction in neutral aqueous solution (k_{uncat}).[52] The proficiency can be also visualized from the free energy profile for the uncatalyzed and enzymatic reactions, as shown in Figure 3.1, where E is enzyme, S is substrate, and P is product. $\Delta G^{\neq}_{uncat}$ is the barrier for the uncatalyzed reaction, while $\Delta G^{\neq}_{cat}$ is the barrier for the reaction catalyzed by enzyme, ΔG_0 is the reaction energy, also called driving force for enzymatic reactions, which is not altered by the presence of the enzyme. $\Delta\Delta G^{\neq}$ represents the catalytic power of enzyme and is related to the proficiency

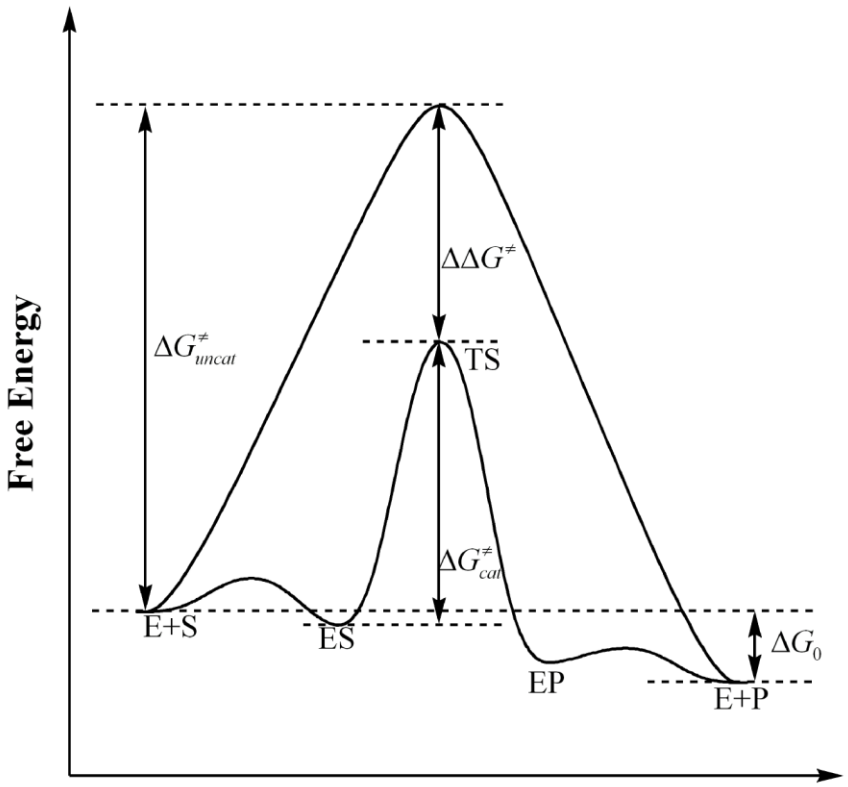

Figure 3.1. *Free energy profile for uncatalyzed and enzymatic reactions.*

(k_{cat}/K_M)k_{uncat}. A transition state (TS) stabilization is achieved by the enzyme. One crucial task of mechanistic exploration of enzymes is to find out how enzyme interacts with their substrates during the reaction pathway, especially in the transition state complex, and why enzyme binds the substrate in the transition state stronger than in the ground state.

One of the most important objectives in enzymology is to understand and explain the catalysis in enzymes. Over the years, many ideas and theories have been put forward. The first hypothesis, offered by Fischer, is the "lock and key" model, which proposed that enzyme can bind and activate the substrate to a reactive conformation.[53] Haldane suggested that "*the key does not fit the lock quite perfectly, but exercises a certain strain on it*", which can be termed "ground state destabilization".[54] In 1948, with the introduction of transition state theory, Pauling proposed that "*enzymes are molecules that are complementary in structure to the activated complexes of the reactions that they catalyze*".[55] This paradigm has been an important guiding principle in drug discovery. Warshel has proposed that electrostatic effects play an important role in enzyme catalysis.[56,57] The active site provides a preorganized polar environment to stabilize the transition state much more than that in water. Several alternative proposals have also been put forward, such as: (a) *ground-state destabilization*[58-63] (b) *dynamical effects*[64-66] (c) *near attack conformations*[67-69] (d) *entropic guidance*[70] (e)

desolvation effects[71] (f) *low-barrier hydrogen bond*[72] (g) *covalent catalysis*[73]. The best way to understand enzyme efficiency is to use a clear energy-based analysis, which must satisfy the laws of physics and chemistry.[56]

3.2 Quantum chemical modeling of enzymes

Quantum chemical methods have been shown to be a very powerful tool in investigating enzymatic pathways, discriminating between different mechanistic proposals, and rationalizing the origin of catalytic power.[39-51] Transition states and intermediates that are difficult to be verified by experiments, can be located and characterized. Potential energy profiles can thus be derived and rate-limiting steps and associated energetic barriers can be obtained. In addition, different reaction pathways can be judged and the feasibility of the reaction pathway can be compared with available experimental kinetic results. Furthermore, the role of various parts in the active site can be analyzed.

Nowadays, there are two common approaches. One is to treat the whole enzyme, which usually contains tens of thousands of atoms. It is impossible to handle such large systems using pure quantum chemical methods. Quantum mechanics and molecular mechanics (QM/MM) combined methods have been developed, in which a relative small part of the active site is treated using quantum mechanics, typically density functional theory or semi-empirical method, the rest is handled with molecular mechanics.[74-85] The alternative one is called the cluster approach, in which a part of the active site is chosen, typically on the order of 100-150 atoms. The selected model resembles the catalytic of the enzyme quite well and can be treated as accurate quantum chemical methods as possible.[39-51]

In this thesis, the cluster approach will be used to investigate the reaction mechanisms of some very difficult enzymatic systems. It has been argued that active site models neglect the effects of the protein environment and the results must be treated very carefully.[86] However, the cluster approach has been developed to become quite robust and accurate. Two approximations are used to account for the surrounding effects. First, the protein matrix can entail steric hindrance on the model, which can be managed by locking certain atoms, usually where the truncations are made. This can easily prevent artificial movements of various groups in the model and keep the optimized structures close to the experimental one. A small model might be too rigid, and the calculated energetics become unreliable. However, by increasing of the model size, more flexibility is introduced and this approximation becomes more and more accurate. Second, the protein surrounding provides electrostatic interactions on the model. The environment can be simply treated as a homogenous polarizable medium

with some dielectric constant. Usually, ε=4 is used and represents the protein surrounding quite well. The solvation energy is calculated as a single-point based on gas phase optimized geometries. It has shown that the solvation effects saturate quickly with the increase of the model size. Systematic studies have shown that the choice of dielectric constant becomes unimportant when the model size approaches 150-200 atoms.[87-90] An example will be given below, namely the study of the decarboxylation step in pyruvate-dependent decarboxylase.

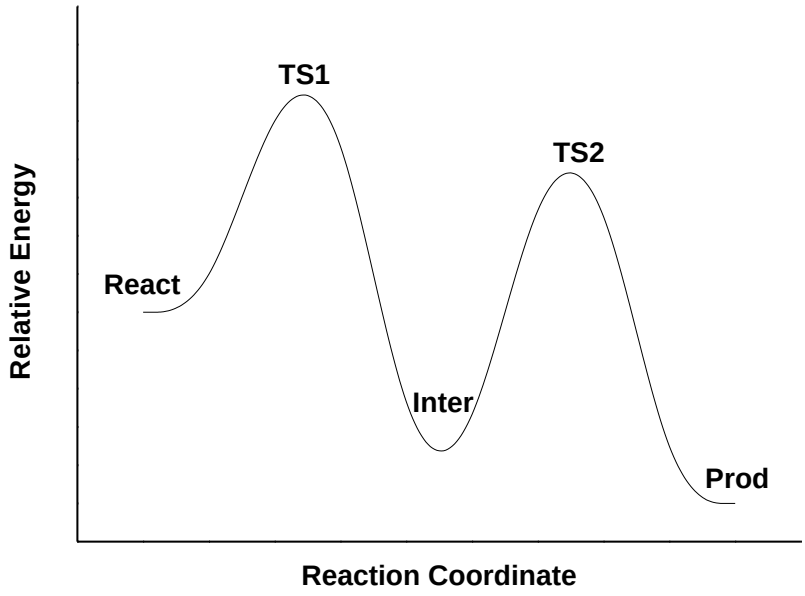

Figure 3.2. *A representative potential energy profile for a two-step reaction with two reaction/catalytic cycle.*

It should be noted that an important effect of the surrounding (including enzyme surrounding) is so-called "friction effect", which doesn't need to be modeled explicitly. However, this is important in analyzing the potential energy profiles for the reactions. With the potential energy profile in **Figure 3.2** as an example, it can be seen that, in gas phase TS1 is rate-limiting step. The reason is that in gas phase, the system keeps its kinetic energy downhill from TS1 to Inter. However, the picture will be different in solution (or in enzyme environment). From TS1 to Inter, the system will instantaneously lose its kinetic energy due to its vibrations and collisions with the surroundings. The system has to accumulate energy again to pass TS2. Therefore, TS2 becomes rate-limiting in solution. This insight is helpful in the analysis of the PES produced in this thesis.

3.2.1 Design of active site model

In the quantum chemical cluster approach, a proper model of the active site first has to be designed to mimic the chemical/catalytic property of the enzyme. For reactions in enzymes, the 3-D structural information about the active site is crucial for understanding the reaction mechanism and the role of various parts. Most mechanistic studies using computational methods are based on available X-ray structures (or solution NMR structures), usually deposited in *Protein Data Bank* (PDB). The PDB files can be visualized using available software, for example, VMD[91] or YASARA[92]. With phospholipase C as an example, the structure of the whole enzyme is shown in **Figure 3.3A** (PDB entry: 2AH7[93]). Important active site residues, cofactors, metal ions, water molecules, and some other important compounds can be extracted from the PDB file (**Figure 3.3B**). To reduce the size of the model, the residues are truncated, so that in principle only their side chains or important peptide backbones are included in the model (**Figure 3.3C**). Hydrogen atoms are added manually. In some cases, the protonation states of aspartates, glutamates, histidines, lysines and arginines are not well-established, thus both protonated and unprotonated ones have to be considered in calculations (see for example the studies on dihydroorotase and human renal dipeptidase (Sections 4.1 and 4.2)). A model substrate is often used if the natural substrate is too large. Several possible binding modes have to be considered, based on available structures of enzyme-substrate complexes or enzyme-inhibitor complexes. However, it should be remembered that the inhibitor binding mode may not reflect the mode for natural substrate (see for example the study on N-acyl homoserine lactonase, section 4.3).[94]

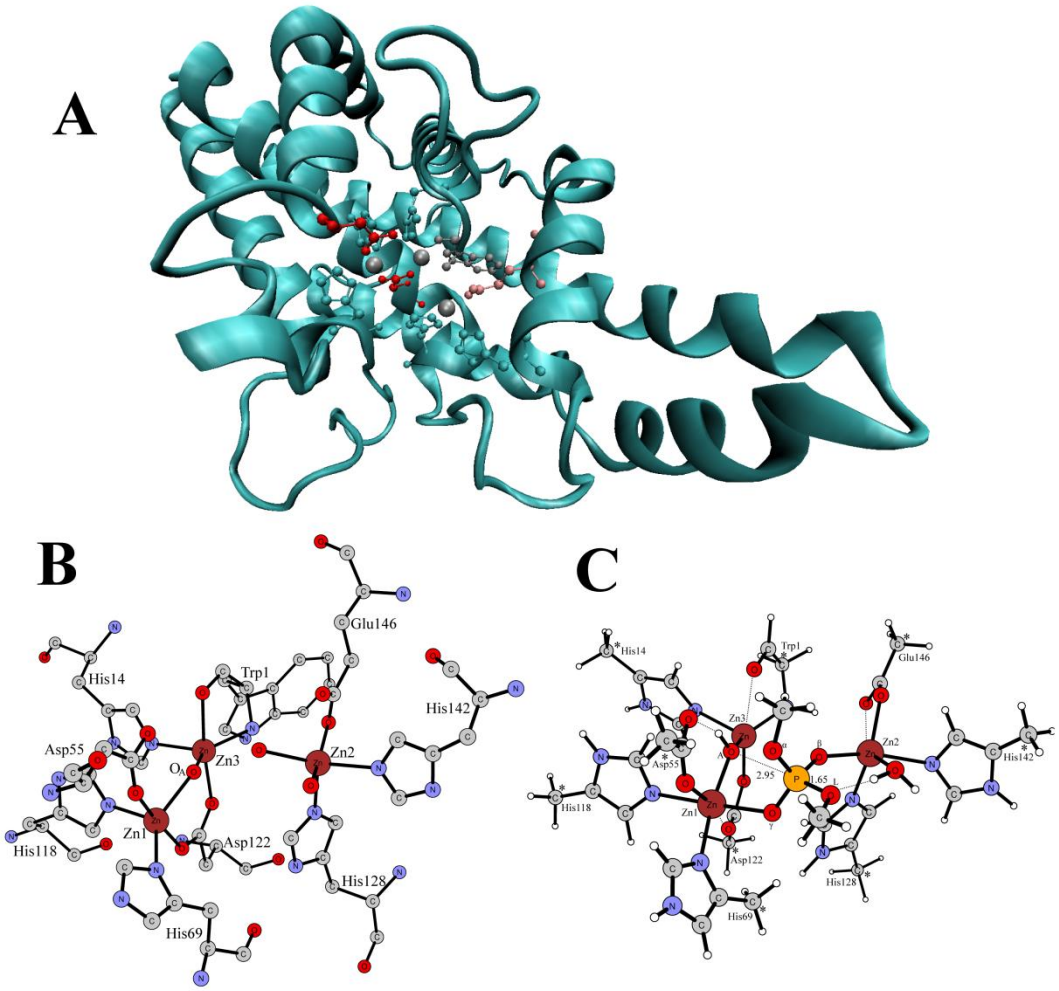

***Figure 3.3**. Example of active site model design, the case of phospholipase C (PDB entry: 2AH7[93]). Important residues together with zinc ions and water were extracted. Residues were truncated and hydrogen atoms were added manually. Asterisks indicate atoms that were fixed at their crystallographically observed positions in the calculations.*

3.2.2 Computational details

Almost all calculations presented in this thesis were carried out using the hybrid functional B3LYP[19,20] as implemented in Gaussian03[95] program package. For geometry optimizations, usually 6-31G(*d,p*) basis sets were used for the C, N, O, H elements, 6-311+G(*d*) for P and S, the LANL2DZ[96] pseudopotential for Zn and the LANL2TZ(*f*)[97] for W. In the studies of phospholipase C (paper V) and nuclease P1 (paper VI), a larger basis sets 6-311+G(*2d,2p*) were used for P and five oxygens around it to ensure a good description of the penta-coordinated species. Based on these optimized geometries, single-point calculations were performed using usually the larger basis sets 6-311+G(*2d,2p*) for C, N, O, P, S, Zn, H atoms and the LANL2TZ(*f*) basis set for W.

The polarization effects of the enzyme environment were considered by performing single-point calculations on the optimized structures at the same theory level as the geometry optimizations using the conductor-like polarizable continuum model (CPCM) method.[98-101] The dielectric constant was typically chosen to be 4.

Analytical frequency calculations were performed at the same level of theory as the geometry optimizations on the stationary points along the reaction pathways, to verify their characters and to estimate the zero-point energy (ZPE) corrections. The locking procedure used in the cluster model leads to a few small imaginary frequencies, typically smaller than 50*i* cm^{-1}. These do not affect the obtained energetic results significantly, but make the calculation of the harmonic entropy effects less accurate. The entropy was thus usually not considered here. In any case, entropy effects are expected to be rather small and do not alter any mechanistic conclusions, as shown, for example, by QM/MM free energy calculations on histone lysine methyltransferase.[102]

In some cases, other functionals or basis sets were used for the sake of evaluating the approach. They are indicated explicitly.

3.2.3 Techniques of locating transition state

The most challenging task in reaction mechanism studies is to find the transition state connecting reactant and product in every step. One simple method is to use the Synchronous Transit-Guided Quasi-Newton method,[103] in which a linear synchronous transit or quadratic synchronous transit approach is applied to guess an initial structure close to the transition state, followed by geometry optimizations with quasi-Newton algorithm. In this method, the reactant and product structures are needed to guess a transition state structure. This method works for some simple reactions, but is not applicable for complex reactions and cannot guarantee that the one found is the right one, which connects the reactant and product. An alternative and more robust method is to select a main reaction coordinate, like bond distances, bond angles, or dihedral angles, followed by a linear transit along this coordinate. An energy profile can be plotted as a function of the reaction coordinate. The one with the highest energy can be used for transition state searching. A Hessian is usually needed for transition state optimizations. The simplest way is to do an analytical frequency calculation to generate the Hessian, at the same theory level of the optimization which is very time consuming for large systems or at a lower level to save some time. The latter one might create problems for large systems, especially for transition state with small imaginary frequency. An alternative choice

is to use the local Hessian, in which the second derivatives of energy with respect to only a few main degrees of freedom are calculated numerically. The transition state optimization can be easily restarted without the need of calculating the Hessian again. This procedure can save a lot of time and has been successfully applied to the location of many transition states.

3.2.4 Convergence of solvation effects (Paper VII)

As mentioned above, previous studies on histone lysine methyltransferase, 4-oxalocrotonate tautomerase, and haloalcohol dehalogenase demonstrated that the solvation effects decrease very quickly with the size of the cluster.[87-89] Here another example is examined to further corroborate this important phenomenon. The specific enzyme is L-Aspartate α-decarboxylase (AspDC), which catalyzes the decarboxylation of L-aspartate to β-alanine (**Scheme 3.1**).[104-108] AspDC belongs to a class of decarboxylases that utilize a pyruvate rather than pyridoxal 5'-phosphate as a cofactor.[106]

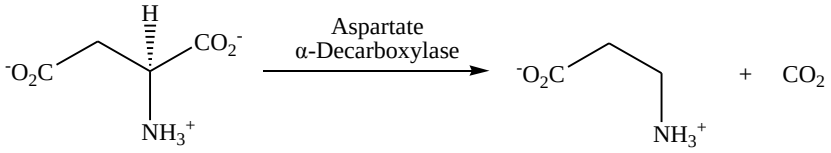

Scheme 3.1. *Reaction catalyzed by AspDC.*

From the crystal structure of AspDC in complex with aspartate amide (PDB code: 1UHE[109]), several models with increasing size have been constructed to evaluate the solvation effects on the barriers and reaction energies for the critical C-C bond cleavage step. A number of dielectric constants, ε=2, 4, 8, 16, and 80, were used. The energies are summarized in **Table 3.1**. The optimized structure of the transition state for **Model V** that has the largest size is shown in **Figure 3.4**.

Table 3.1*. Summary of the calculated energetics for the various models of AspDC (kcal/mol).*

	Model 0 27 atoms		Model I 76 atoms		Model II 95 atoms		Model III 135 atoms		Model IV.1 166 atoms		Model IV.2 189 atoms		Model V 220 atoms	
	Barrier	Reaction Energy	Barrier	Reaction energy	Barrier	Reaction energy	Barrier	Reaction energy	Barrier	Reaction energy	Barrier	Reaction energy	Barrier	Reaction energy
Cluster	0.1	-9.5	8.3	0.3	8.8	-0.6	9.0	0.8	13.9	9.9	13.0	4.2	13.5	9.0
ε=2	2.3	-5.7	12.0	2.9	11.9	2.6	11.4	2.5	13.1	8.7	15.6	7.7	13.5	9.6
ε=4	3.7	-3.5	14.2	4.5	13.6	4.5	12.9	3.5	12.7	8.0	17.0	9.8	13.4	9.9
ε=8	4.5	-2.2	15.5	5.5	14.7	5.6	13.5	4.1	12.5	7.6	17.8	9.9	13.3	10.0
ε=16	4.9	-1.5	16.1	6.0	15.3	6.2	13.9	4.3	12.4	7.4	18.2	10.5	13.3	10.0
ε=80	5.2	-1.0	16.7	6.5	15.7	6.7	14.2	4.6	12.3	7.2	18.5	10.9	13.3	10.0

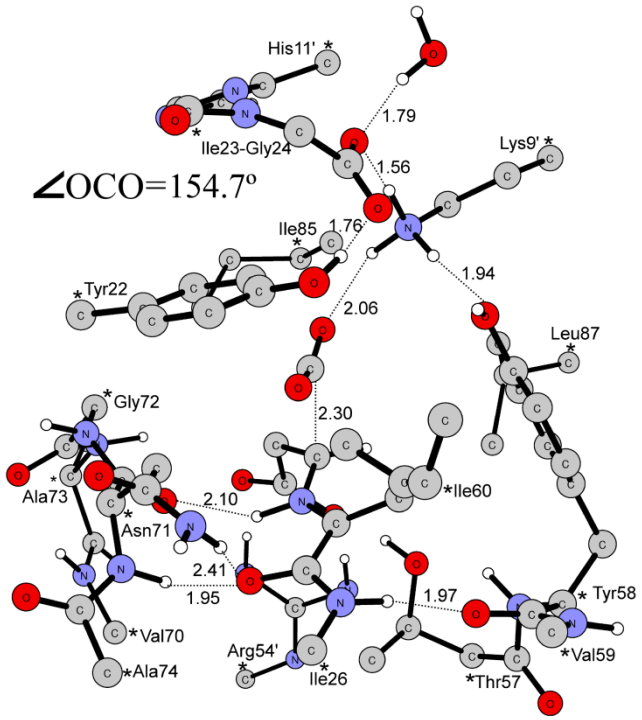

***Figure 3.4**. Optimized structure of the transition state for **Model V**. Asterisks indicate atoms that were fixed at their crystallographically observed positions in the calculations. Many hydrogen atoms are omitted for clarity.*

First, only a pyruvoyl group is included to form a covalent bond to the substrate, and no surrounding residues are included. The carboxylate is thus exposed to the solvent in the CPCM calculations. The solvation effects with ε=80 are calculated to be +5.1 and +8.5 kcal/mol for the barrier and reaction energy, respectively.

For active site models, with the increase of the model size, the solvation effects in general decrease somewhat. For the barrier, we can see that the solvation effects are +8.4, +6.9, +5.2, -1.6, and -0.2 kcal/mol, respectively, for **Model I**, **II**, **III**, **IV.1**, and **V**, respectively.

***Table 3.2**. Summary of calculated dipole moment (D) and volume ($Å^3$) for the various models of AspDC.*

	dipole moment						volume					
	I	II	III	IV	IV’	V	I	II	III	IV	IV’	V
Reactant	26.1	21.7	28.6	25.6	32.0	25.9	794.3	995.1	1368.5	1708.5	1990.4	2335.2
TS	17.3	14.9	23.5	20.5	23.8	23.8	796.6	1006.3	1372.4	1718.1	1983.0	2345.8
Product	13.0	13.8	22.3	20.0	22.9	22.0	812.4	1026.3	1389.5	1717.5	1973.9	2346.9

The Onsager dipole model[110,111] can be used to analyze the relationship between the solvation effects and the cluster size. In this model, the electrostatic contribution to the

solvation free energy is proportional to the square of dipole moment for dipole in a spherical cavity and inverse proportional to the volume.

$$\Delta G_{elec} = -\frac{\varepsilon - 1}{2\varepsilon + 1}\frac{\mu^2}{a^3} \quad (3\text{-}1)$$

According to Onsager's dipole model, for a fixed dipole, when the volume is doubled, the solvation energy becomes one half. This indicates that when the model size increases, the solvation effects on the barrier and reaction energy become less and less important. The calculated dipole moment and volume for various cluster models are shown in **Table 3.2**. It can be seen that for all models, the reactant has larger dipole moment than the transition state and product, indicating larger solvation effects in the reactant. In addition, the dipole moment difference between reactant and product decreases with the increase of the model size with the exception of **Model IV.2**, which might explain the unexpected increase of solvation effects from **Model III** to **Model IV.2**. With the increase of the model size, the substrate is well-solvated and the dipole moment changes less and less, leading thus to saturation of solvation effects.

The volume of a model increases with the increase of its size. The change of volume from reactant to product decreases with the increase of the model size, since a large model is capable of accommodating the structural changes during the reaction.

3.3 Transition state theory

Classical transition state theory (TST),[112] developed by Eyring, Polanyi, and Evans, is a statistical mechanical theory of reaction rate constants, widely used in the interpretation of reactivity of chemical processes. The theory was derived based on the following assumptions: (1) there exists a hypersurface which divides space into a reactant region and a product region with a transition state structure lying at the lowest point on this surface, and trajectories from reactant region passing through this dividing surface in the products direction will not come back. (2) the distribution of energy in the reactant region and the transition state follows the Boltzmann distribution law, which means the transition state species are in equilibrium with reactants. (3) the nuclear motion along the reaction coordinate is electronically adiabatic and can be described by classical mechanics.[113] The reaction rate constant (k) can then be expressed as:

$$k = \frac{k_B T}{h} e^{-\Delta G^{\neq}/RT} \quad (3\text{-}2)$$

where k_B is the Boltzmann's constant (1.38×10^{-23} $J\ K^{-1}$) and h is the Plank's constant (6.626×10^{-34} $J\ s$), $\Delta G^{\neq}$ is the Gibbs free energy change from reactant to transition state, R is the gas constant (8.314 $J\ K^{-1}\ mol^{-1}$) and T is the absolute temperature in Kelvin. At room temperature (298.15 K), a rate constant of 1 s^{-1} corresponds to a barrier of 17.4 kcal/mol, and an increase of $\Delta G^{\neq}$ by 1.4 kcal/mol leads to a decrease by one order of magnitude in reaction rate constant. For enzymatic reactions, the calculated reaction barrier can be compared with the experimental kinetic results, if k_{cat} is available. A too high calculated barrier (larger than 25 kcal/mol) often implies that either the mechanism is wrong or that the model is missing something or contains some artifacts.

Generally, the free energy barrier ($\Delta G^{\neq} = \Delta H^{\neq} - T\Delta S^{\neq}$)is used to derive the reaction rate constant according to eq. (3-2). However, in this work only the enthalpy part $\Delta H^{\neq}$ is considered. As we discussed before, the entropy cannot be calculated accurately with the cluster model. This approximation works very well for the systems studied in the present thesis, because the entropy effect is believed to be quite small.

Chapter 4

Dinuclear zinc enzymes

In this chapter, four dinuclear zinc enzymes are investigated using the quantum chemical cluster approach. These are two members of the amidohydrolase superfamily, dihydroorotase (DHO) and human renal dipeptidase (hrDP), and two members of the metallo-β-lactamase superfamily, N-acyl homoserine lactonase hydrolase (AHL lactonase) and RNase Z. The reactions catalyzed by these enzymes are shown in **Scheme 4.1**.

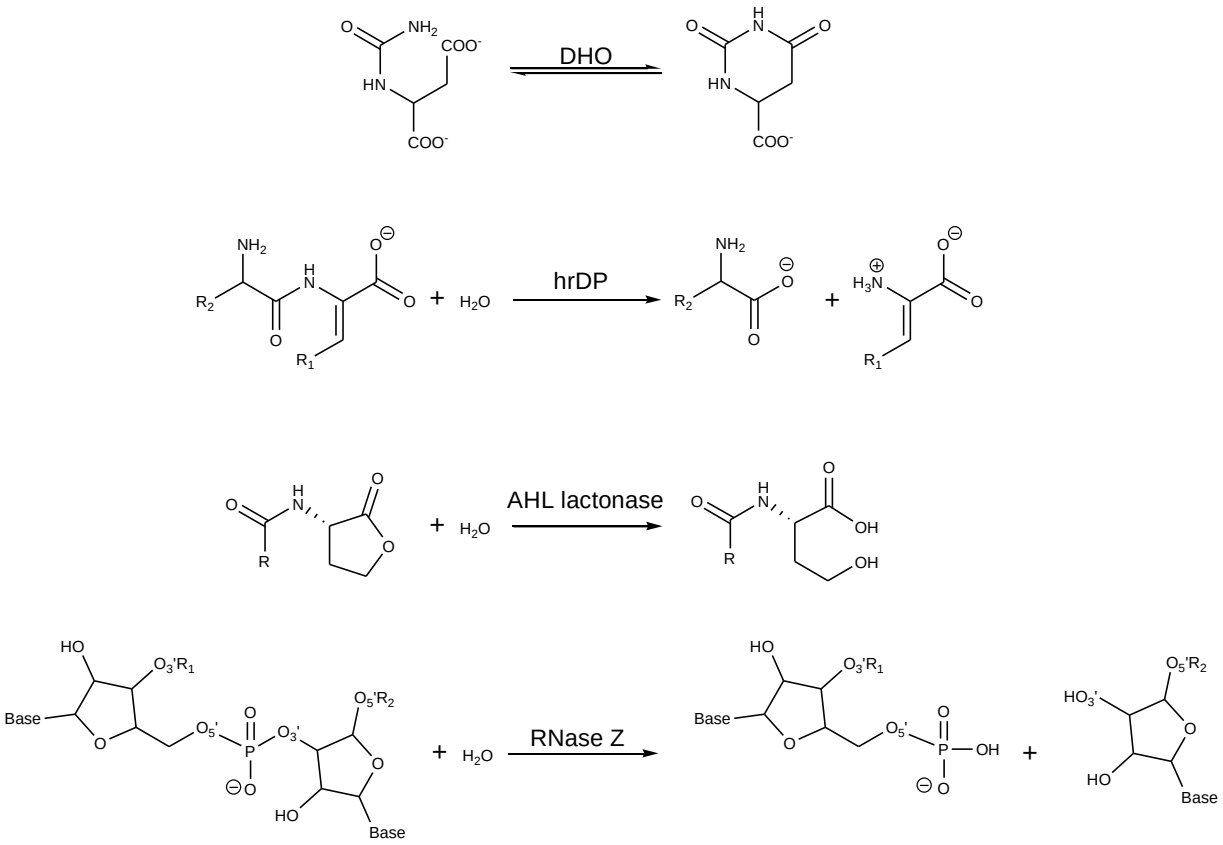

Scheme 4.1. *Reactions catalyzed by DHO, hrDP, AHL lactonase, and RNase Z.*

For DHO and hrDP, the different protonation states of a key residue in the active site are considered. For AHL lactonase, two possible substrate binding modes are taken into account. The reaction mechanisms are studied and the role of zinc ions and other important residues is analyzed.

4.1 Dihydroorotase (Paper I)

DHO catalyzes the reversible interconversion of dihydroorotate and carbamoyl aspartate (**Scheme 4.1**).[114-117] The crystal structure of DHO from *Escherichia coli* has been solved with a dinuclear zinc site.[118,119] Interestingly, dihydroorotate was found bound to the active site of one monomeric unit of the dimeric protein while carbamoyl aspartate was bound to the adjacent monomer. In the monomer with dihydroorotate bound, the two zinc ions are bridged by an oxygen species and a carboxylated lysine (Kcx102), and the amide carbonyl oxygen of dihydroorotate is orientated toward Zn_{β}. In addition, the α-carboxylate group of dihydroorotate forms hydrogen bonds to the side chains of Arg20, Asn44, and His254.

From our calculations, it was found that the bridging oxygen species is a hydroxide. When a water molecule was used for geometry optimizations, a proton transfer from this bridging water to Asp250 takes place automatically. Three second shell residues, Arg20, Asn44, and His254 bind the α-carboxylate group of dihydroorotate through four hydrogen bonds. No significant interaction is observed between the substrate and the zinc ions.

When Asp250 is ionized, the whole reaction proceeds through three steps (**Scheme 4.2**). The optimized transition states are shown in **Figure 4.1**. The reaction initiates from a nucleophilic attack on the substrate carbonyl carbon by the bridging hydroxide directly from its bridging position (**TS1**), without the need of becoming terminal. This attack results in the formation of an oxyanion, stabilized by direct binding to Zn_{β}. In the following step (**TS2**), a proton transfer takes place from the bridging hydroxyl group to Asp250, coupled with a rotation of the latter to form a hydrogen bond to the amide nitrogen, which becomes ready for protonation. Our calculations show that the protonation step (**TS3**) is in concomitant with C-N bond cleavage. This step is calculated to be the rate-limiting step, with an accumulated barrier of 19.7 kcal/mol (**Figure 4.2**). Thus Asp250 catalyze the reaction by functioning as a bridge to transfer a proton from the bridging hydroxyl group to the amide nitrogen.

When Asp250 is neutral, the entire reaction takes place in one single concerted step (**TS-pt**, **Figure 4.1**). The bridging hydroxide performs the nucleophilic attack on the amide carbonyl carbon, in contaminant with proton transfer from Asp250 to amide nitrogen and C-N bond cleavage. The barrier for this mechanism is calculated to be 34.0 kcal/mol. In the reactant complex, beside the bridging hydroxide, the dinuclear zinc cluster has only one more negative ligand, Kcx102. The total charge of the model is +2. The nucleophilicity of the bridging hydroxide is strongly lowered by the two zinc ions, and thus is not sufficient enough to perform an attack. Therefore a high barrier is associated with a neutral Asp250 residue.

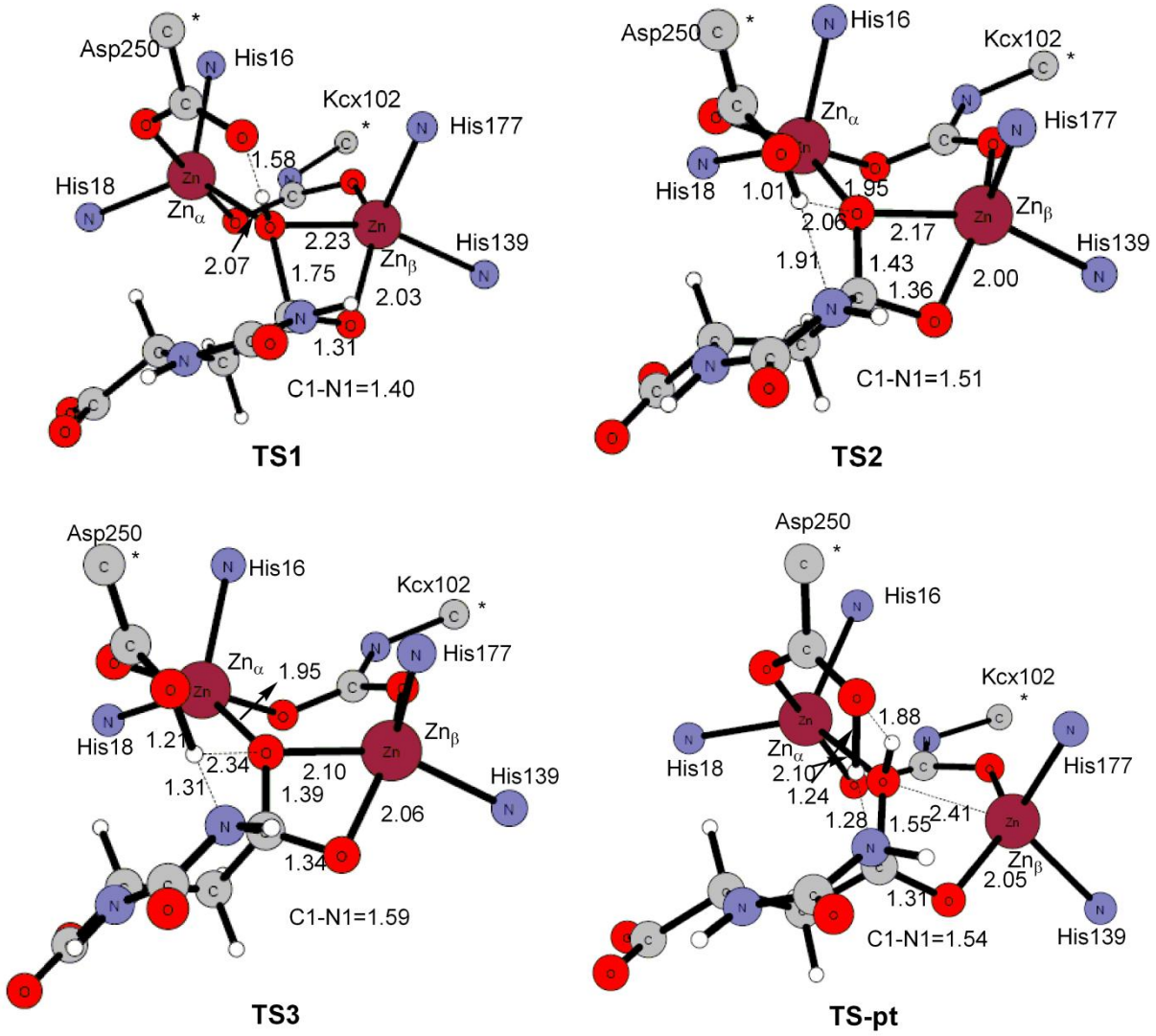

Figure 4.1. *Optimized geometries of the transition states along the reaction pathway with ionized and protonated Asp250. For clarity, Arg20, Asn44, and His254, the histidine rings, and some hydrogen atoms are omitted.*

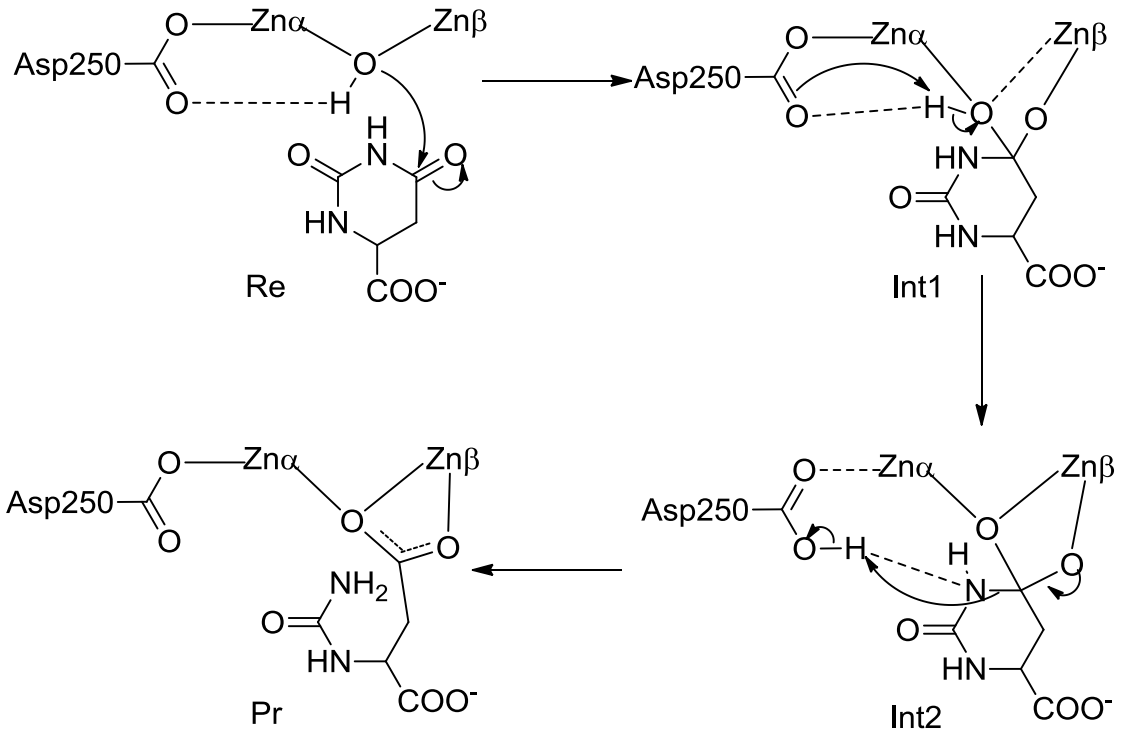

Scheme 4.2. *Reaction mechanism of enzymatic interconversion of dihydroorotate and carbamoyl aspartate suggested from the calculations.*

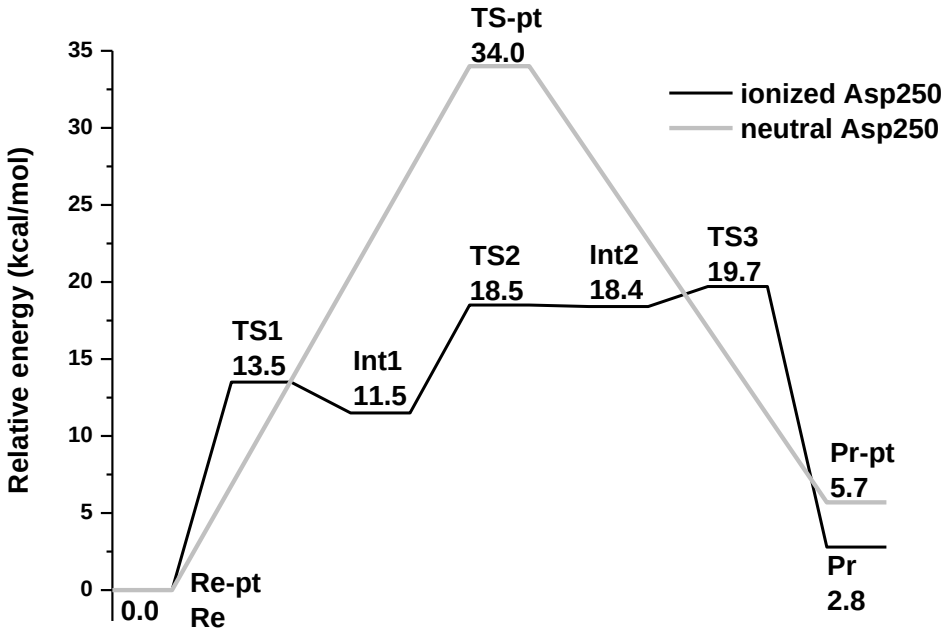

Figure 4.2.*Calculated potential energy profile for the hydrolysis of dihydroorotate by dihydroorotase with ionized and neutral Asp250.*

4.2 Human renal dipeptidase (Paper IV)

HrDP catalyzes the hydrolysis of dipeptides with $_{D-}$, $_{L-}$, or dehydro-amino acids at the C-terminus (**Scheme 4.1**).[120-122] It plays an important role in the renal metabolism of glutathione and leukotriene D4 and the hydrolysis of β-lactam antibiotics.[123-125] The crystal structure of hrDP (PDB code: 1ITU[126]) has been solved in both the unliganded form and in complex with the dipeptidyl moiety of a cilastatin inhibitor, which can be used as a probe for colon cancer.[127,128] The two zinc ions are bridged by Glu215 and an oxygen species, which is hydrogen-bonded to Asp288. A second-shell residue, His152, forms one hydrogen bond to the peptide carbonyl oxygen. In addition, the carboxylate terminus of the inhibitor is coordinated to Zn2 and hydrogen-bonded to Arg230 and Tyr255.

Similar to DHO,[129] the critical residue in the active site, Asp288, was considered to be both neutral and ionized. However, both cases give quite feasible barriers and thus the protonation state of Asp288 is not important to the catalysis.

The substrate binds into the di-zinc center in a bidentate fashion, in which the N-terminal amino group is coordinated to Zn1, while the C-terminal carboxylate is coordinated to Zn2. The lack of Zn1-amino group interaction seems to account for the inactivation of cilastatin. In addition, this interaction might be a common feature for dinuclear zinc aminopeptidases, as suggested in aminopeptidase from *Aeromonas proteolytica*,[130,131] methionine aminopeptidase from *Escherichia coli*,[132] and bovine lens leucine aminopeptidase.[133]

When Asp288 is neutral, the first step (**TS1, Figure 4.3**) is a nucleophilic attack by the bridging hydroxide on the peptide carbonyl carbon, affording a tetrahedral intermediate with its oxyanion stabilized by Zn2. Since there are three negatively-charged ligands bound to the two zinc ions (bridging hydroxide, Asp22 and Glu125), the nucleophilicity of the bridging hydroxide is sufficient enough for the attack, which is different from the case in DHO as discussed above (When Asp250 is neutral). In the subsequent step (**TS2, Figure 4.3**), Asp288 functions as a bridge to shuttle a proton from the bridging hydroxyl group to the peptide nitrogen, coupled with the C-N bond cleavage. The role of Asp288 is thus quite similar to that of Asp250 in DHO. Both steps have quite feasible barriers (around 10 kcal/mol, **Figure 4.4**).

When Asp288 is ionized, the first nucleophilic attack step (**TS1', Figure 4.3**) is similar to the neutral Asp288 case. Since Asp288 does not coordinate to Zn2, its protonation state thus has small influence on this step. The barriers are quite close for these two cases (neutral and ionized Asp288). Different from that in neutral Asp288 case, calculations with ionized

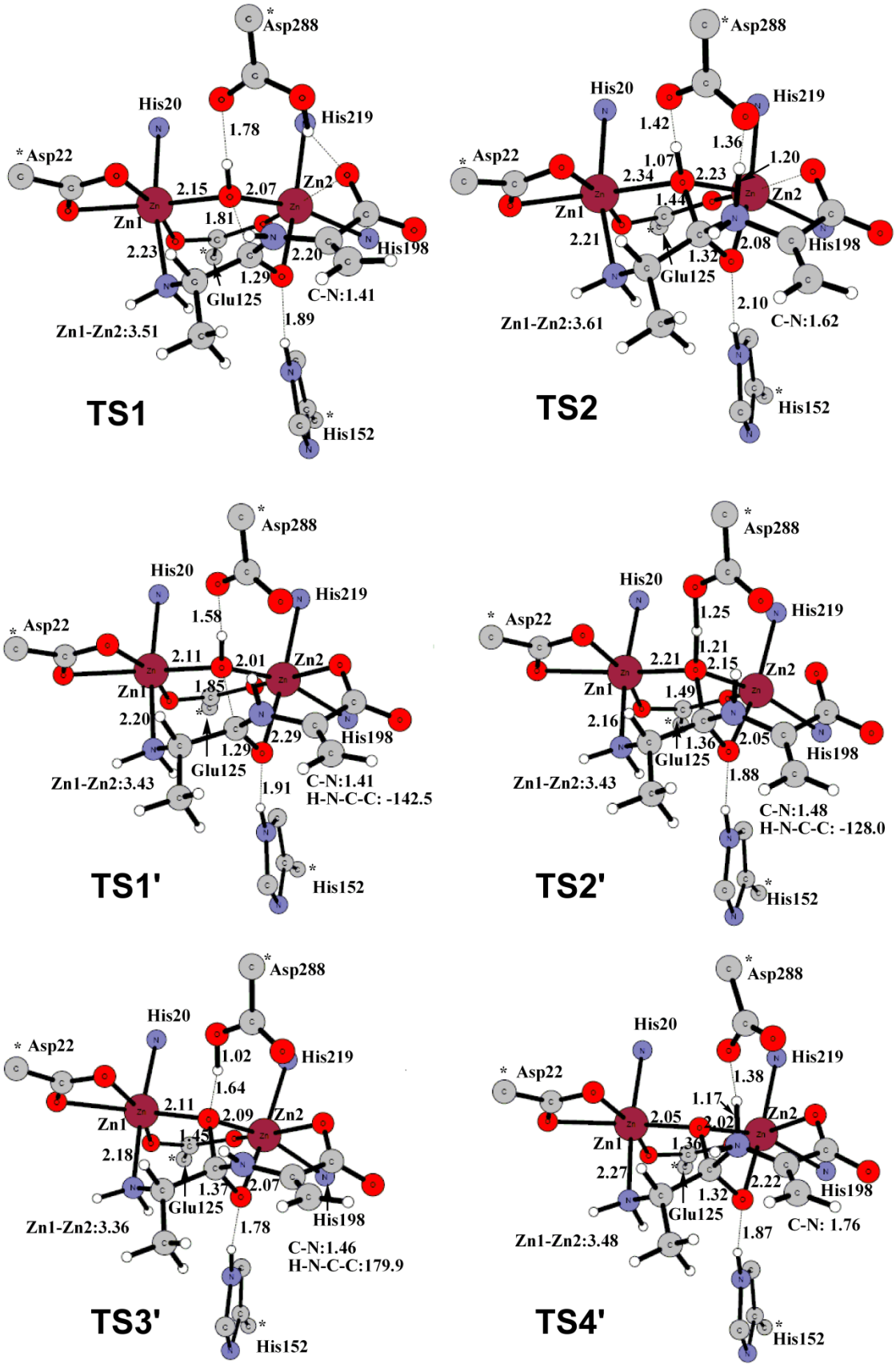

***Figure 4.3**. Optimized geometries of the transition states along the reaction pathway with neutral (TS1 and TS2) and ionized (TS1' to TS4') Asp288.*

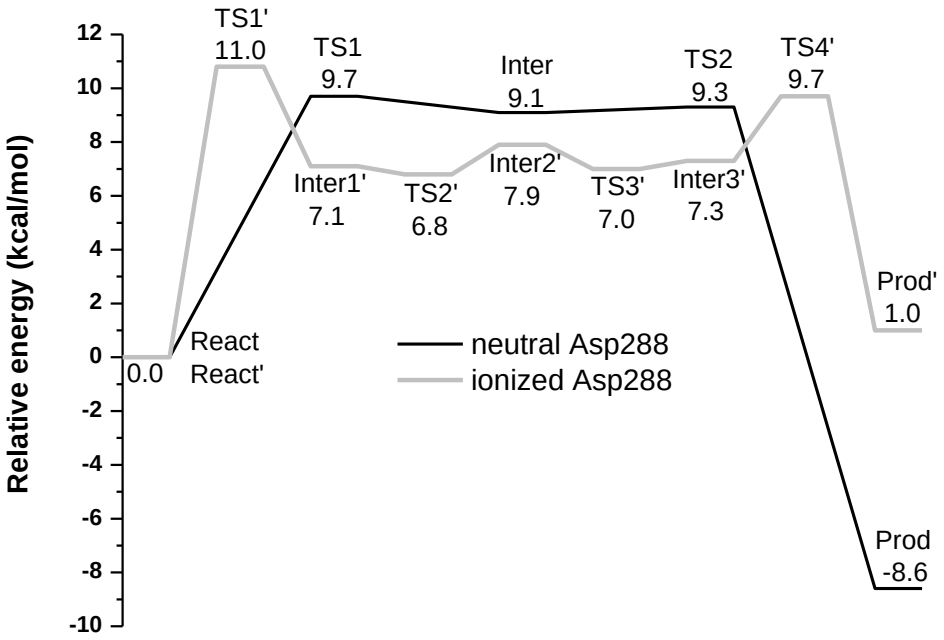

Figure 4.4*.Calculated potential energy profile for the hydrolysis of dehydro Ala-Ala dipeptide by hrDP with ionized and neutral Asp250.*

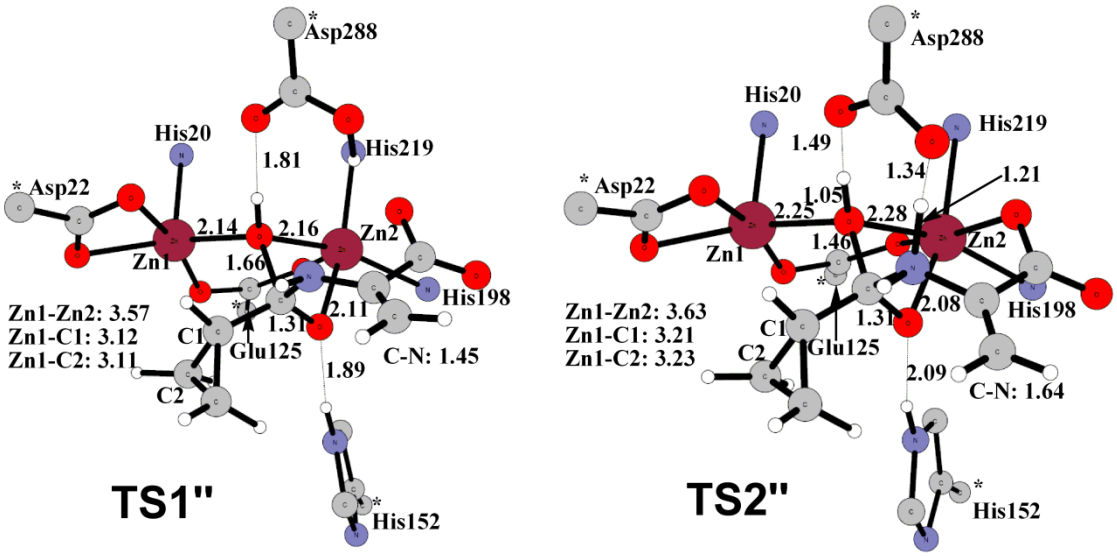

Figure 4.5*. Optimized geometries of the transition states along the reaction pathway for cilastatin hydrolysis.*

Asp288 suggest that two more steps are needed for the product formation from the tetrahedral intermediate. First, the proton transfers from the bridging hydroxyl group to Asp288 (**TS2',**

Figure 4.3), followed by cleavage of hydrogen bond between the Asp288 oxygen and peptide NH and the inversion of the configuration of the peptide nitrogen (**TS3', Figure 4.3**). Finally, the protonated Asp288 donates a proton to the peptide nitrogen, in contaminant with the C-N bond cleavage. These three steps have quite low barriers. From **Figure 4.4**, we can see that both cases give quite feasible barrier for the dipeptide hydrolysis.

Based on our suggested mechanism, the reactivity of cilastatin was also investigated using the same active site model to understand the inactivity of this inhibitor. A neutral Asp288 is considered here. The mechanism was found to be very similar to that for natural substrate hydrolysis (transition states shown in **Figure 4.5**). However, the barriers +for the two steps are significantly higher (15.6 and 15.9 kcal/mol for the first and second step). The main reason comes from the repulsion between Zn1 and the cyclopropyl group of cilastatin.

4.3 N-acyl homoserine lactone hydrolase (Paper II)

N-acyl homoserine lactones (AHLs) are extracellular signaling molecules for bacteria.[134,135] N-acyl homoserine lactone hydrolase can impede AHL activity by catalyzing the hydrolytic ring opening of AHL (**Scheme 4.1**).[136-139] AHL lactonase from *Bacillus thuringiensis* belongs to the metallo-β-lactamase superfamily.[140] The crystal structure of AHL lactonase shows that in the active site, the two zinc ions are bridged by Asp191 and an oxygen species, most likely a hydroxide.[141,142] In addition, Asp108 is coordinated to Zn2. Homoserine lactone was found to be a reversible inhibitor and bound into the active site though interactions of its carbonyl oxygen with Zn2 and its ring oxygen with Zn1. An alternative substrate orientation in which the role of the two zinc ions switches was also suggested based on enzyme product structure and QM/MM molecular dynamics simulations.[143,144] Here we calculated the potential energy profiles for these two substrate orientations.

The first-shell environment of the two zinc ions in AHL lactonase is quite similar to that of DHO, which has a bridging hydroxide and two negatively-charged residues. Therefore, an ionized Asp108 was used, which is believed to be the active form. The total charge of the dinuclear zinc center is +1. The substrate binding mode (orientation A) suggested from enzyme product complex was considered first. No interactions can be observed between the two zinc ions and the substrate. Similar to the two aforementioned dinuclear zinc enzymes, the bridging hydroxide performs a nucleophilic attack on the ester carbonyl carbon (**A-TS1, Figure 4.6**), resulting in the formation of a tetrahedral intermediate, stabilized by Zn1. A

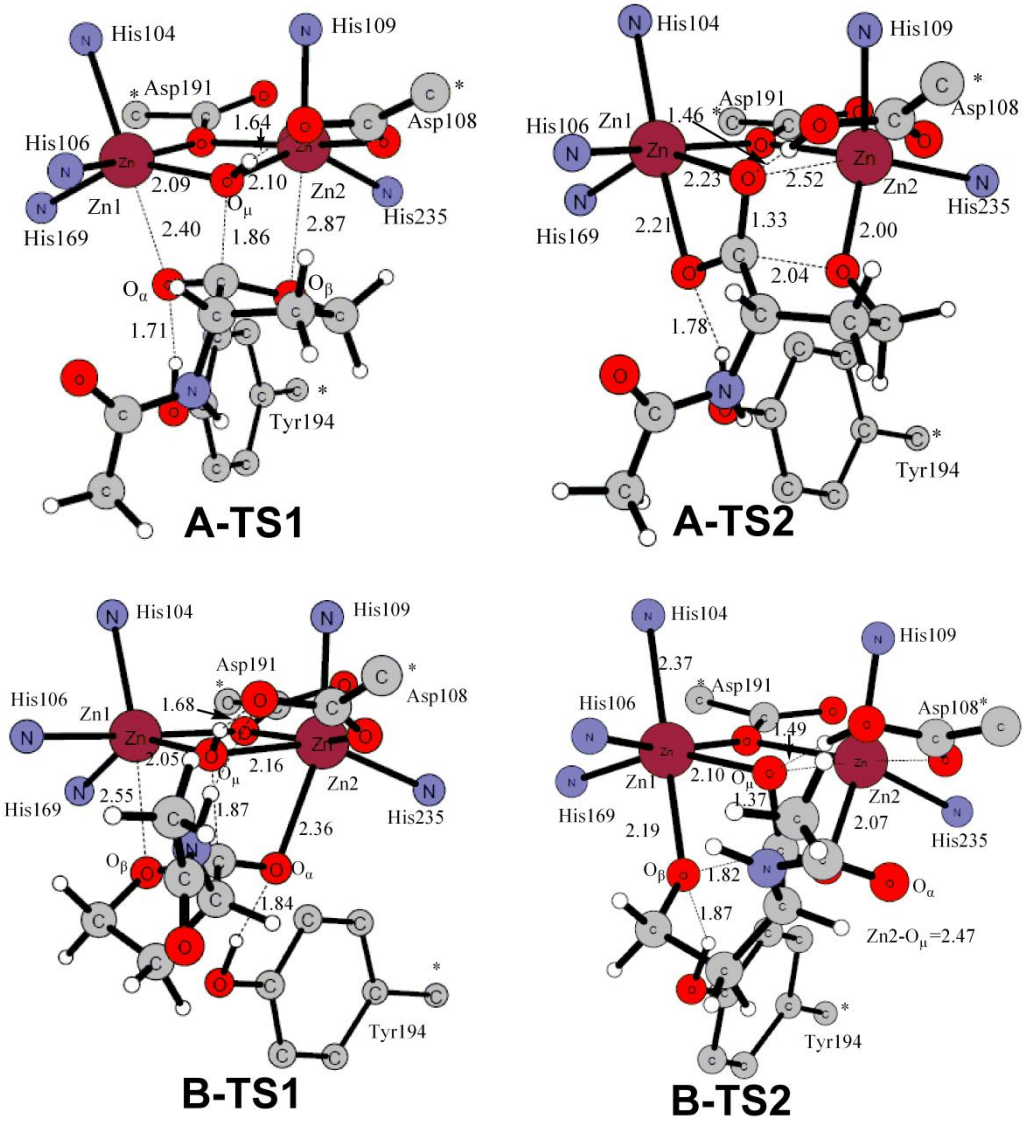

Figure 4.6*. Optimized geometries of the transition states along the reaction pathway by AHL lactonase in two different substrate orientations.*

second shell residue Tyr194 also provides stabilization on the intermediate through hydrogen bonding interaction. This is then followed by the ring C-O bond cleavage (**A-TS2, Figure 4.6**), facilitated by Zn2 which provides electrostatic stabilization on the emerging alkoxide. The barriers for these two steps are quite close (16.4 and 17.0 kcal/mol for **A-TS1** and **A-TS2**, respectively, **Figure 4.7**) and thus we cannot distinguish which one of them is rate-limiting. However, the fact that the second step has a slightly higher barrier is consistent with experimental suggestion from thio-effect studies. The mechanism for this substrate orientation is summarized in **Scheme 4.3**.

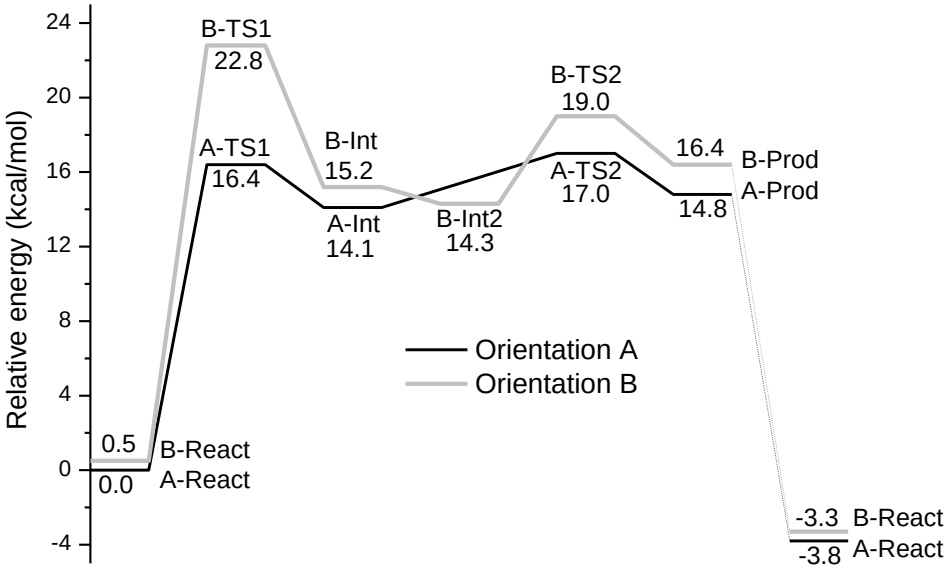

***Figure 4.7**. Calculated potential energy profiles for N-acyl-L-homoserine lactone hydrolysis in the two different substrate orientations.*

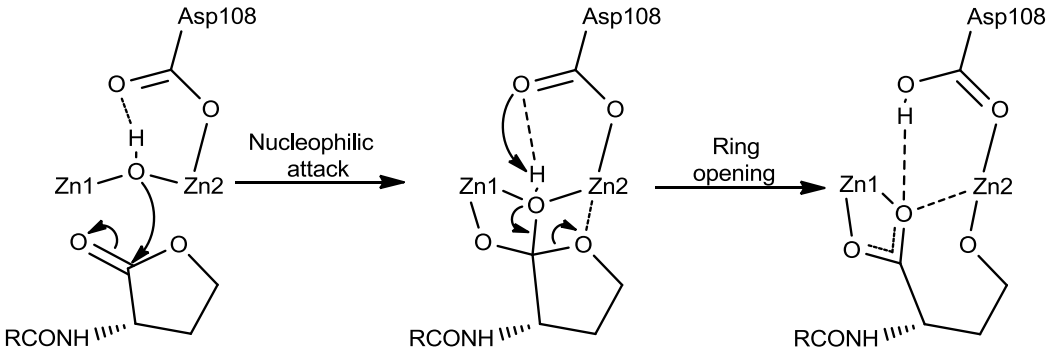

***Scheme 4.3**. Reaction mechanism of AHL lactonase.*

Next we optimized all stationary points for the other substrate orientation (orientation B). The reactant complex has slightly higher energy (+0.5 kcal/mol) than that in orientation A. The mechanism is quite similar. However, the role of the two zinc ions switches and the barrier for the two steps becomes different. In the nucleophilic attack step (**B-TS1**), Zn2 now stabilizes the oxyanion. Since Zn2 has one more negatively-charged ligand compared to Zn1, Zn2 is slightly less positively-charged and Zn1 works thus better in stabilizing the oxyanion. Similar results have been observed in DHO and hrDP, as shown above.[129,145] This might be extended to other dinuclear zinc hydrolases that the more positively charged Zn is selected to stabilize the oxyanion in the tetrahedral intermediate. The barrier now is 22.3 kcal/mol (**Figure 4.7**), 5.9 kcal/mol higher than that in the other orientation. The following ring

opening step (**B-TS2**) now is facilitated by Zn1, with a barrier of 19.0 kcal/mol. In this substrate orientation, the nucleophilic attack is rate-limiting. The high barrier explains why the homoserine lactone inhibitor is not hydrolyzed.

4.4 RNase Z (Paper III)

RNase Z is a endoribonuclease that catalyzes the hydrolysis of 3'extremities of tRNA.[146-149] Similar to AHL lactonase, it belongs to the metallo-β-lactamase superfamily.[150] The crystal structure of *Bacillus subtilis* RNase Z reveals that the two zinc ions in the active site are bridged by Asp211 and an oxygen species, presumably a hydroxide.[151-155] In addition, Asp67 coordinates to Zn_{β} and a Glu231-His247 diad is located close to the dinuclear zinc site. The total charge of the two zinc ions together with their first-shell ligands is +1. His247 forms a hydrogen bond to the zinc bound phosphate. Mutational studies suggest that the Glu-His diad may act as a general acid to protonate the leaving group.[156-159]

The phosphate group of the substrate that takes one negative charge coordinates to the two zinc ions with its two oxygen atoms. In addition, His247 offers a hydrogen bond to the leaving oxygen. Calculations show a two-step mechanism for the RNA hydrolysis (**Scheme 4.4**). Similar to the three enzymes discussed above,[129,145,160] the bridging hydroxide performs a nucleophilic attack on the phosphate center (**TS1**, **Figure 4.8**), in concerted with the departure of the leaving group, which takes a proton from the Glu-His diad. Downhill from **TS1**, a proton transfer from the bridging hydroxide to Asp67 takes place. **TS1** is characterized to be associative and has a barrier of 13.6 kcal/mol (**Figure 4.9**). This step is calculated to be exothermic by 6.6 kcal/mol. The resulting alcohol can be easily released to the solution by breaking its hydrogen bond to His247. The direct release of the phosphomonoester will require much more energy due to its strong interaction with the two zinc ions. An alternative choice is that a water molecule that displays the leaving alcohol makes the reverse attack on the phosphorus center regenerating the bridging hydroxide. This looks like a mirror image for the first step. The exchange energy for alcohol by water in the intermediate complex is calculated to be exothermic by 4.7 kcal/mol and thus the energy of **Inter2** was set to be -11.3 kcal/mol. Now the Glu-His diad acts as a general base to take a proton from the water molecule, thus generating a hydroxide to perform the reverse attack. The barrier for this step is calculated to be 18.1 kcal/mol, which is rate-limiting for the whole reaction. This step is endothermic by 7.9 kcal/mol. From **Prod**, the phosphate can be released and a new substrate can dock into the dinuclear zinc site for the next catalytic cycle.

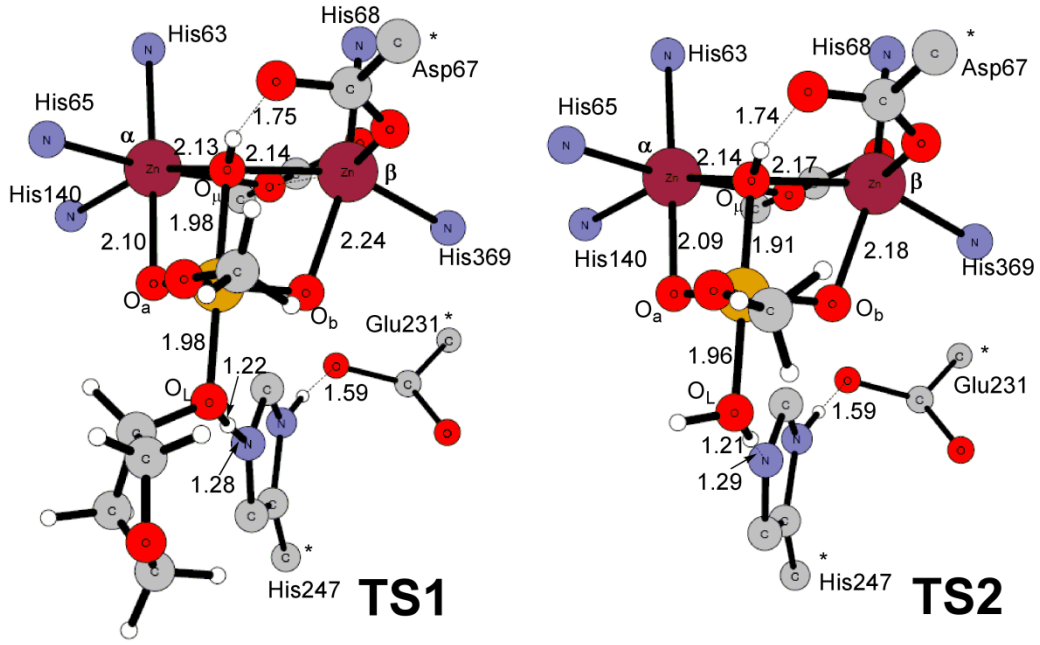

***Figure 4.8**. Optimized geometries of the transition states along the reaction pathway by RNase Z.*

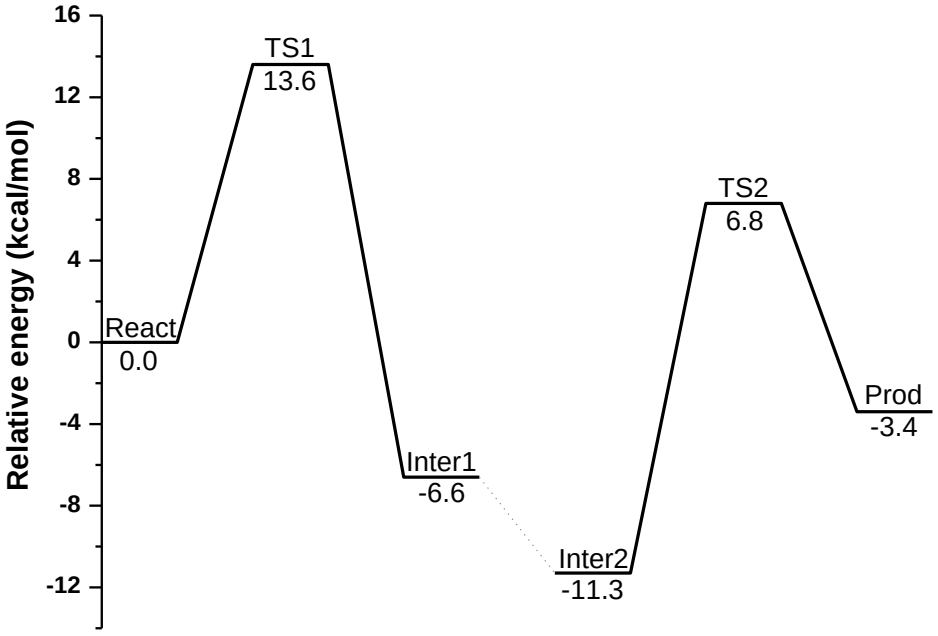

***Figure 4.9**. Calculated potential energy profiles for RNA hydrolysis by RNase Z.*

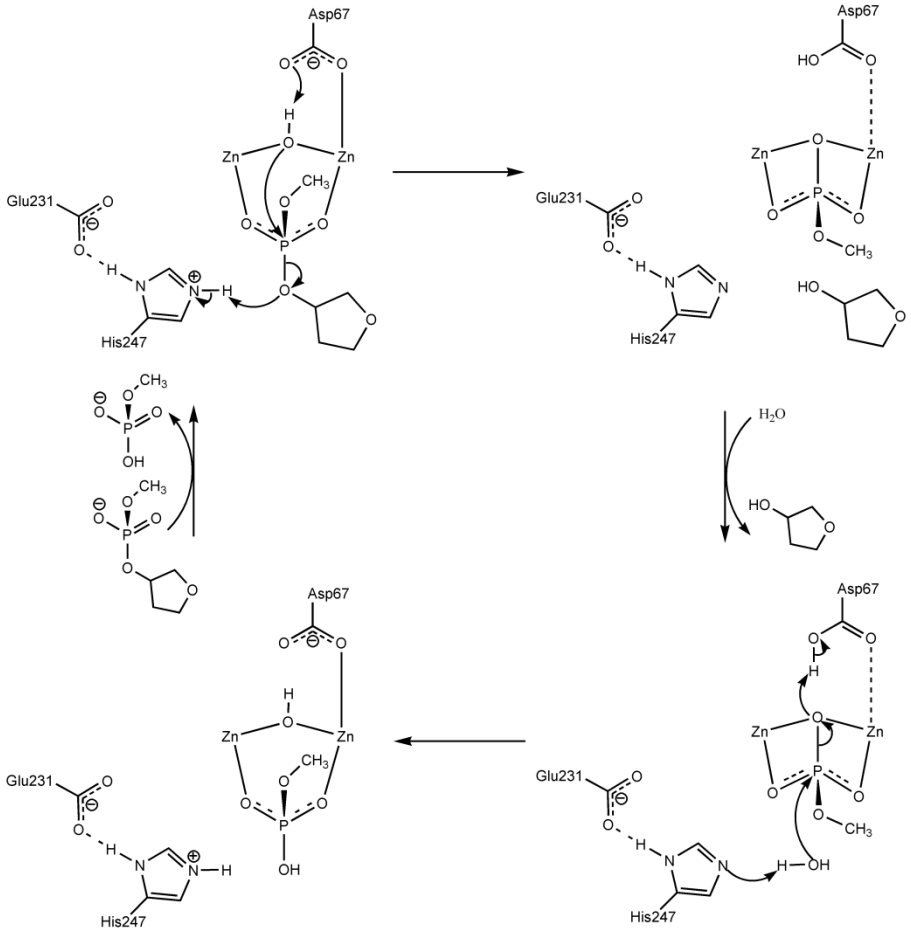

***Scheme 4.4**. Suggested RNA hydrolysis mechanism by RNase Z.*

Chapter 5

Trinuclear zinc enzymes

There are three known enzymes that utilize three zinc ions for their catalytic activity, namely Phospholipase C (PLC), Nuclease P1 (NP1), and Endonuclease IV. All of them catalyze the hydrolysis of phosphate. It is not clear why these enzymes need one more zinc ion compared to dinuclear zinc enzymes and what the role of this additional zinc ion is.

Here the mechanism of PLC and NP1 are investigated. The reactions catalyzed by these two enzymes are shown in **Scheme 5.1**. For PLC, the two mechanistic proposals in which either a Zn-bound water or a bridging hydroxide was believed to be the nucleophile are verified. For NP1, both the phosphomonoesterase and phosphodiesterase activity are studied. These results are compared with dinuclear zinc enzymes studied.

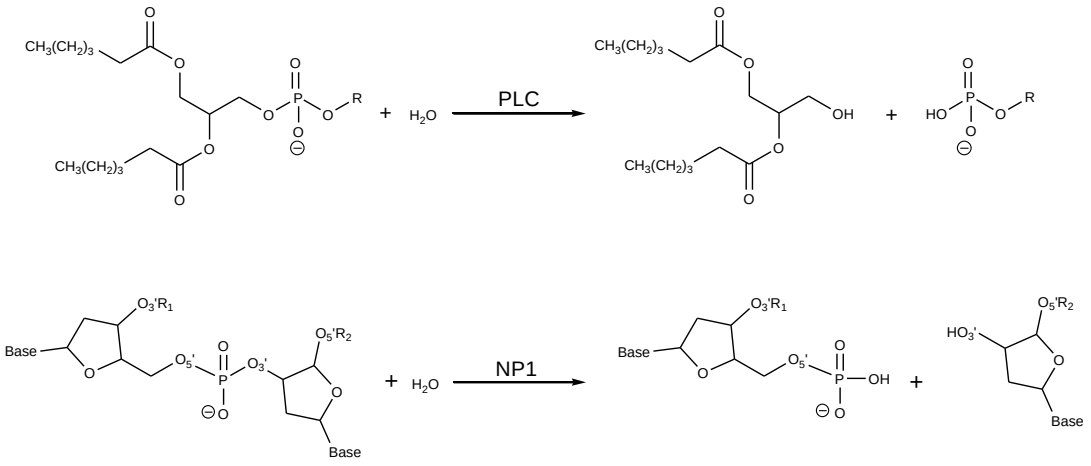

Scheme 5.1. *Reaction catalyzed by PLC and NP1.*

5.1 Phospholipase C (Paper V)

PLC is a phosphodiesterase and catalyzes the hydrolysis of phospholipids, yielding a secondary messenger diacylglycerol and a phosphorylated headgroup (**Scheme 5.1**).[161-166] In *Bacillus cereus*, the phosphatidylcholine-preferring PLC (PLC_{BC}) is an extracellular monomeric enzyme containing 245 residues.[167] Its crystal structure has been solved and revealed a trinuclear zinc center in the active site.[167] Zn1 and Zn3 are bridged by Asp122 and

an oxygen species, while Zn2 is bridged to Zn3 through an oxygen species. In addition, Zn1 coordinates to Asp55, His69 and His118, and Zn2 is ligated by His128, His142 and Glu146, and Zn3 is bound to Trp1, and His14.

The mechanism of PLC was not well understood and two scenarios have been suggested based on different substrate bind modes.[168-172] One proposal is that the substrate phosphate oxygen displaces the bridging hydroxide and a Zn1-bound water molecule performs a nucleophilic attack on the phosphate.[168-171] The other suggestion is that the bridging hydroxide is the nucleophile, similar to many other dinuclear zinc enzymes.[172] Thus the main task here is to identify the nucleophile and the substrate binding mode, as well as the role of the three zinc ions.

5.1.1 Terminal water molecule as nucleophile

When the bridging hydroxide is replaced by one of the phosphate oxygens, the only candidate for the nucleophilic attack is a terminal water molecule that is activated by Zn1. Asp55 takes a proton from the water molecule to generate a hydroxide that performs the attack from the adjacent position to the leaving group. The transition state structure (**A-TS**) is shown in **Figure 5.1**. The barrier is calculated to be 23.8 kcal/mol (**Figure 5.2**), which is higher than the experimental estimates. A berry pseudorotation[173] can be observed to be part of the concerted transition state. The nucleophilic attack results in the direct elimination of an alcohol via a concerted proton transfer from the attack hydroxide to the leaving alkoxide, affording the product complex. The large exothermicity in this mechanism implies that the product release requires quite a lot of energy. A More O'Ferrall Jencks plot[174,175] (**Figure 5.3**) reveals that this concerted transition state has a slightly associative character.

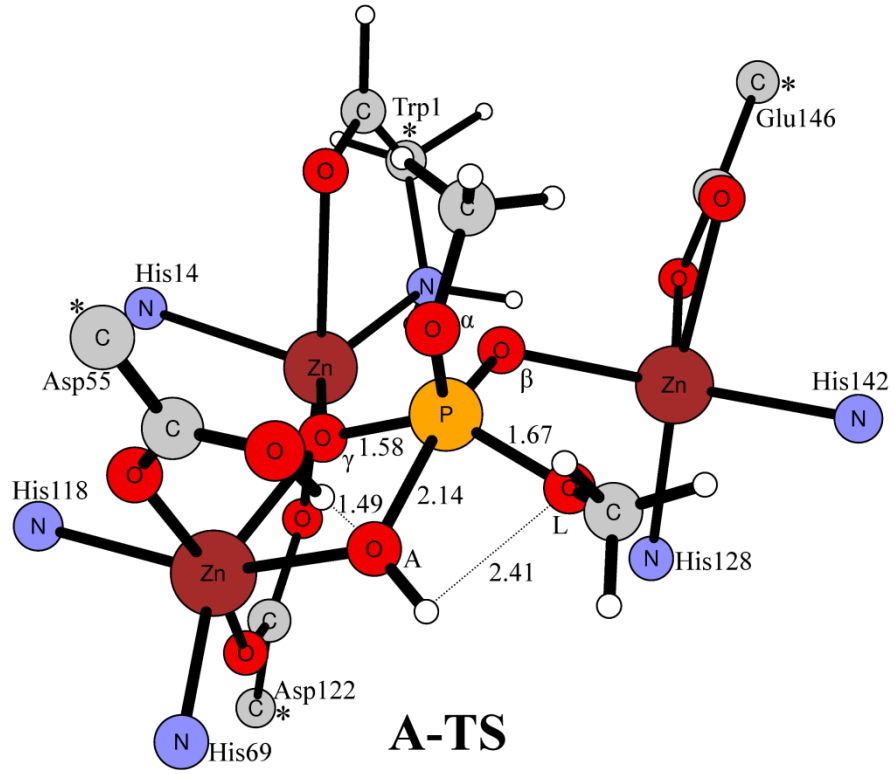

Figure 5.1. *Optimized transition state for terminal water attack mechanism.*

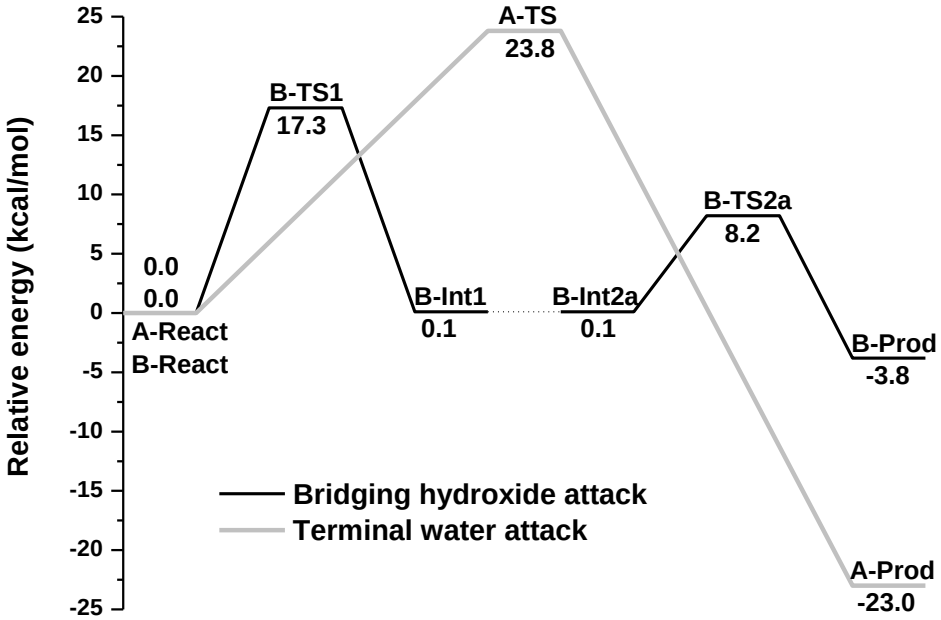

Figure 5.2. *Calculated potential profiles for phosphodiester hydrolysis by phospholipase C in both terminal water attack and bridging hydroxide attack mechanisms.*

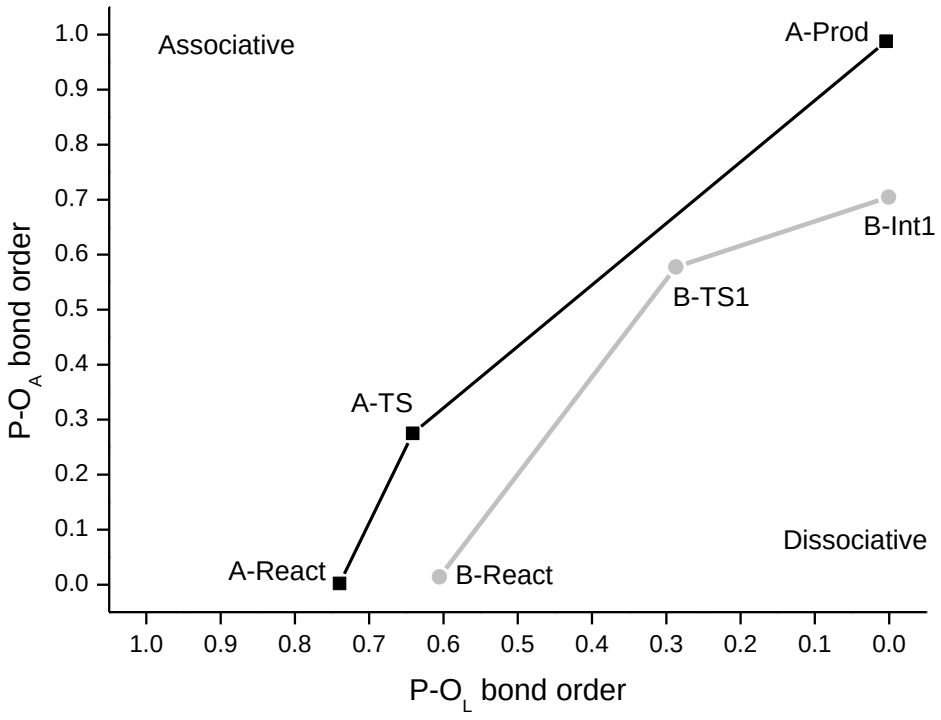

***Figure 5.3**. O'Ferral Jencks (MFJ) plot for terminal water molecule attack mechanism.*

5.1.2 Bridging hydroxide as nucleophile

The above water attack mechanism is associated with a quite high barrier, and the alternative bridging hydroxide attack mechanism was investigated. In this mechanism, a water molecule was added to coordinate to Zn2 and donate a hydrogen bond to the leaving oxygen.

Similar to RNase Z,[176] the bridging hydroxide performs an in-line attack on the phosphate substrate, with inversion of the configuration at the phosphorus center from **B-React** to **B-Int1** via **B-TS1** (**Figure 5.4**). This step is calculated to be rate-limiting, with a barrier of 17.3 kcal/mol, which is 6.5 kcal/mol lower than that in the water attack mechanism. At **B-TS1**, Zn2 activates the bound water molecule as a general acid to offer a proton to the leaving group, facilitating its release. In addition, the other proton transfer takes place from the bridging hydroxide to Asp55, similar to that in RNase Z.[176] It seems that a negative charged species is preferred in the bridging position. The MFJ analysis (**Figure 5.3**) shows that **B-TS1** is slightly associative.

The departure of the leaving alcohol is followed by its release, which is energetically quite fast since it is only hydrogen-bonded to the newly formed Zn2 bound hydroxide. To start a new catalytic cycle, the bridging hydroxide needs to be regenerated. The direct release the phosphate from the tri-zinc center is unlikely due to the tight binding. The alternative

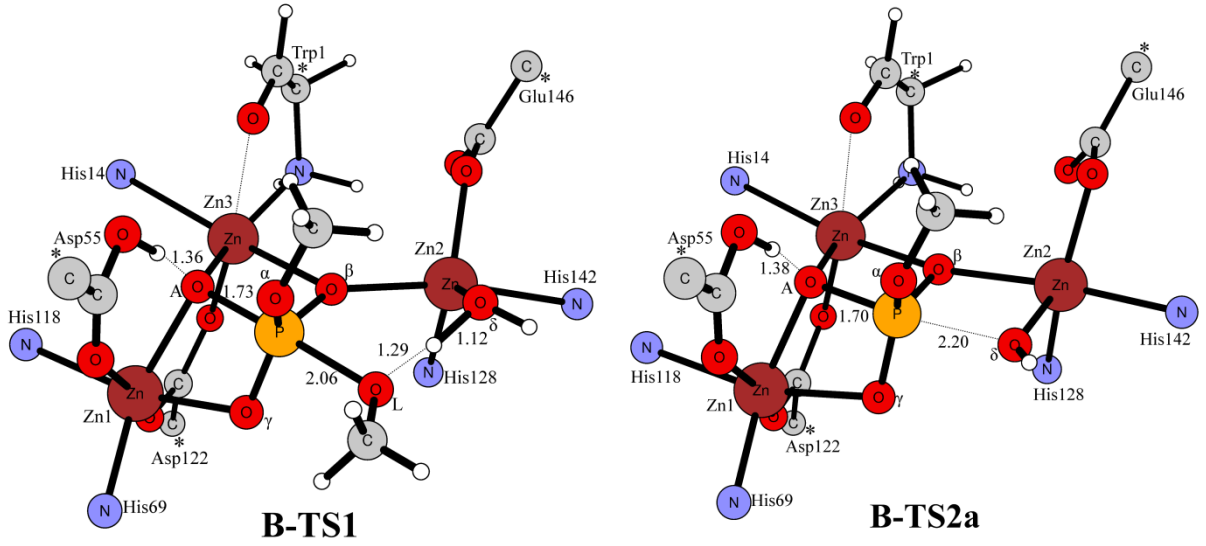

***Figure5.4**. Optimized transition states for bridging hydroxide attack mechanism.*

scenarios are that either the newly generated Zn2 bound hydroxide acts as a nucleophile to reverse the reaction, or this hydroxide acts as a base to activate a water molecule to attack the phosphate. The nucleophilic attack by Zn2 bound hydroxide (**B-TS2a**, **Figure 5.4**) is associated with a barrier of only 8.1 kcal/mol relative to **B-Int2a**. The barrier for the water attack is 18.9 kcal/mol, indicating that there is no need of an additional water molecule for the reaction here. In this second step, Asp55 acts as a general acid to donate a proton to regenerate the bridging hydroxide, which is similar to the function of Asp67 in RNase Z. This also explains why its mutation is associated with a 10^6-fold decrease in activity.[177]

As shown in **Figure 5.2**, the bridging hydroxide attack mechanism is energetically more favorable than the terminal water attack mechanism. Here we can see another evidence for the bridging hydroxide attack mechanism. A deuterium isotope effect of 1.9 has been measured for this enzyme.[178] We simply computed the ZPE difference to derive the isotope effect. For the bridging hydroxide attack mechanism, the calculations yield a normal isotope effect of 2.2, while for the terminal water attack mechanism, the isotope effect is 1.04. These findings further corroborate the results discussed above.

5.2 Nuclease P1 (Paper VI)

Nuclease P1 (NP1) from *Penicillium citrinum* belongs to the zinc-dependent extracellular endonuclease family and serves as a phosphodiesterase to cleave the P-$O_{3'}$ bond of single-stranded DNA and RNA with inversion of the configuration at the phosphorus center.[179-188] It

can also catalyze the removing of the 3'-terminal phosphate group, thus functions as a phosphomonoesterase.[183,184]

The X-ray structure of NP1 (PDB code: 1AK0[189]) reveals almost identical disposition and coordination of the three zinc ions in the active site as PLC. Zn1 is coordinated by Asp45, His60, and His116; Zn2 is bound to His126, His149 and Asp153; while Zn3 is ligated by Trp1 and His6. Zn1 and Zn3 are bridged by Asp120. In addition, it is believed that these two zinc ions are bridged by a hydroxide based on the similarity with the PLC_{BC} active site. A second-shell residue, Arg48, is proposed to interact with the phosphate group of the substrate. A product analogue, dithiophosphorylated oligonucleotide d[A(pS2)T(pS2)T(pS2)T] is located in the active site, with its terminal hydroxyl group bound to Zn2.

The bridging hydroxide is suggested to act as a nucleophile making an in-line attack on the phosphorus center, resulting in inversion of the configuration at the phosphorus center.[189] Zn2 plays a crucial role in stabilizing the leaving oxyanion.

5.2.1 Phosphomonoester hydrolysis

The phosphomonoester substrate binds into the active site through coordination to all three zinc ions and hydrogen bonding to Arg48. After binding, the hydroxide bridging Zn1 and Zn3 is well-arranged for an in-line attack on the phosphorus center. This hydroxide then performs the nucleophilic attack directly from its bridging position, similarly to PLC_{BC}.[190] The optimized transition state ($\mathbf{TS_{Mono}}$) is shown in **Figure 5.5**. Asp45 acts as a general base to accept a proton from the bridging hydroxide, in a similar fashion as the aspartate residue in PLC_{BC} (Asp55) and RNase Z (Asp67). The P-O_L bond cleavage and the nucleophilic attack are found to take place in one concerted step. The barrier is calculated to be 7.2 kcal/mol (**Figure 5.6**). From the structure of $\mathbf{TS_{Mono}}$, we can see that all three zinc ions provide electrostatic stabilization to the penta-coordinated transition state. Zn2 stabilizes the leaving oxyanion, indicating that it can dissociate without the need of protonation. In addition, Arg48 forms stronger hydrogen bonds with the two phosphate oxygens in the transition state compared to the reactant structure, implying that this residue also plays an important role in lowering the barrier. The reaction results in an inversion of the configuration at the phosphorus center, which has also been observed experimentally, it is thus possible that the product is released at this stage.

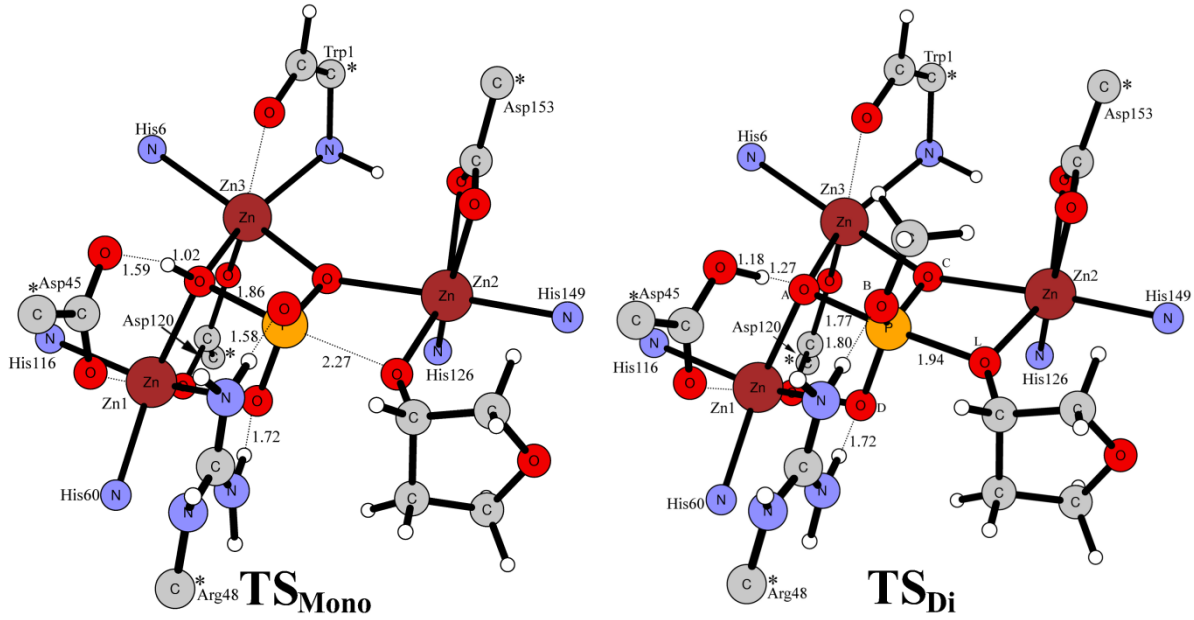

***Figure5.5**. Optimized transition states for phosphomonoester and phosphodiester hydrolysis by NP1.*

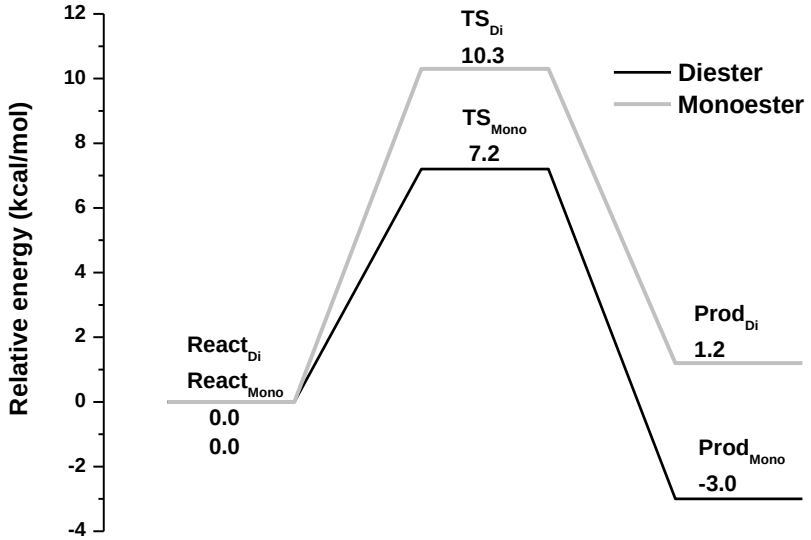

***Figure 5.6**. Calculated potential energy profiles for phosphomonoester and phosphodiester hydrolysis by NP1.*

5.2.1 Phosphodiester hydrolysis

Similarly to the hydrolysis of phosphomonoester, the phosphodiester hydrolysis is also found to proceed through a concerted transition state (**TS_{Di}**, **Figure 5.5**). The energetic barrier is calculated to be 10.3 kcal/mol (**Figure 5.6**), which is somewhat higher than that for phosphomonoester hydrolysis. One reason could be that Arg48 provides better stabilization to

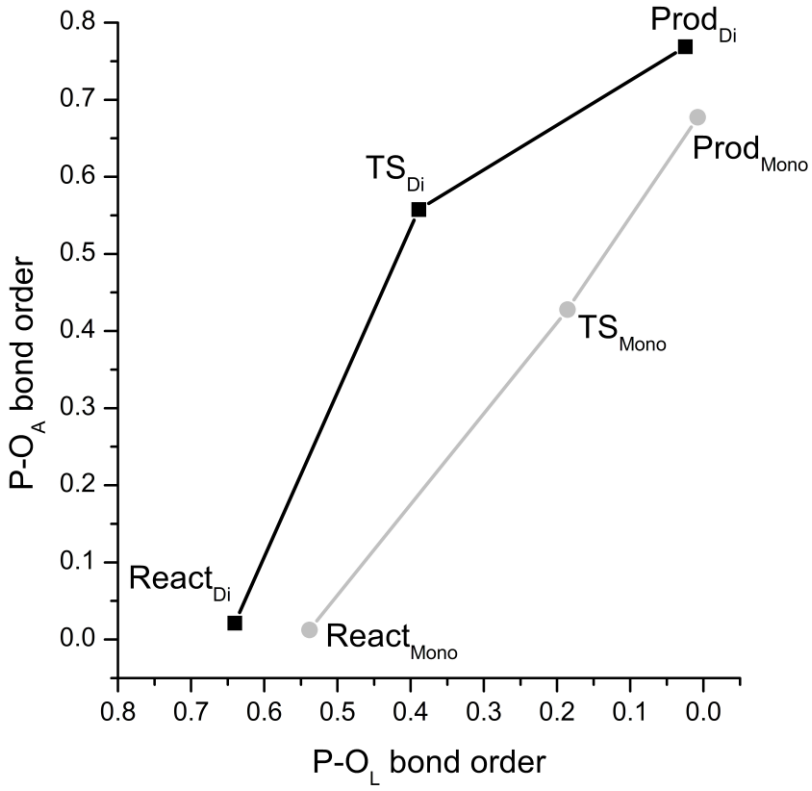

Figure 5.7. *More O'Ferral Jencks (MFJ) plot for phosphomonoester and phosphodiester hydrolysis by NP1.*

the doubly anionic monoester substrate. A similar case has been found in alkaline phosphatase, which utilizes two zinc ions and an arginine residue for phosphate substrate binding, with preference for phosphomonoesters.[191] The reaction is calculated to be endothermic by 1.2 kcal/mol.

The nature of the two transition states are analyzed from a More O'Ferrall-Jencks plot. From **Figure 5.7**, we can see that the concerted transition state for phosphate monoester hydrolysis is quite synchronous, while for diester hydrolysis, it has a more associative character.

Chapter 7

Tungsten-dependent enzymes

Tungsten is the heaviest chemical elements in biology, and has been shown to play essentials roles in biological carbon, nitrogen, and sulfur metabolisms.[192-199] Three different families have been idenfied for tungsten dependent enzymes: aldehyde oxidoreductase, formate dehydrogenase, and acetylene hydratase.[192] The former two families catalyze redox reactions, while the latter catalyzes a non-redox hydration of acetylene.

In this chapter, the mechanism of formaldehyde ferredoxin oxidoreductase (FOR) and acetylene hydratase (AH) are studied. For FOR, four plausible mechanistic scenarios are taken into account to locate the most feasible one. For AH, the protonation state of an important second-shell residue Asp13 being ionized or neutral is considered. A new mechanism is suggested from our calculations.

6.1 Formaldehyde ferredoxin oxidoreductase (Paper VIII)

FOR from *Pyrococcus furiosus* is a tungsten-dependent enzyme that catalyzes the oxidation of formaldehyde to formic acid.[200] Crystal structure analysis shows that in the active site a tungsten ion is bound to two pterin cofactors and an oxygen species, presumably an oxo group.[201] An additional water molecule has been suggested to be coordinated to W.[201] Glu308, a second-shell residue, forms two hydrogen bonds to Tyr416 and the Ser414-Gly415 peptide backbone. In addition, His437 donates hydrogen bond to the dithiolene sulfur anion and forms an additional hydrogen bond to Ser414.

Glu308 is proposed to activate a water molecule to attack the substrate carbonyl group to form a tetrahedral intermediate.[201] In the second step, a hydride transfer to W^{VI}=O occurs, coupled with two electron transfer to W center to generate W^{IV}. The two electrons are then transferred to the ferredoxin cofactors, regenerating the W^{VI} species.

In order to locate an energetically plausible reaction pathway, several mechanistic scenarios were considered in this study. They are labeled as pathway **A**, **B**, **C**, and **D** as shown in **Scheme 6.1**. Pathway **A** is the previously suggested one based on experimental studies, while pathway **B**, **C**, and **D** are new proposals made based on our calculations.

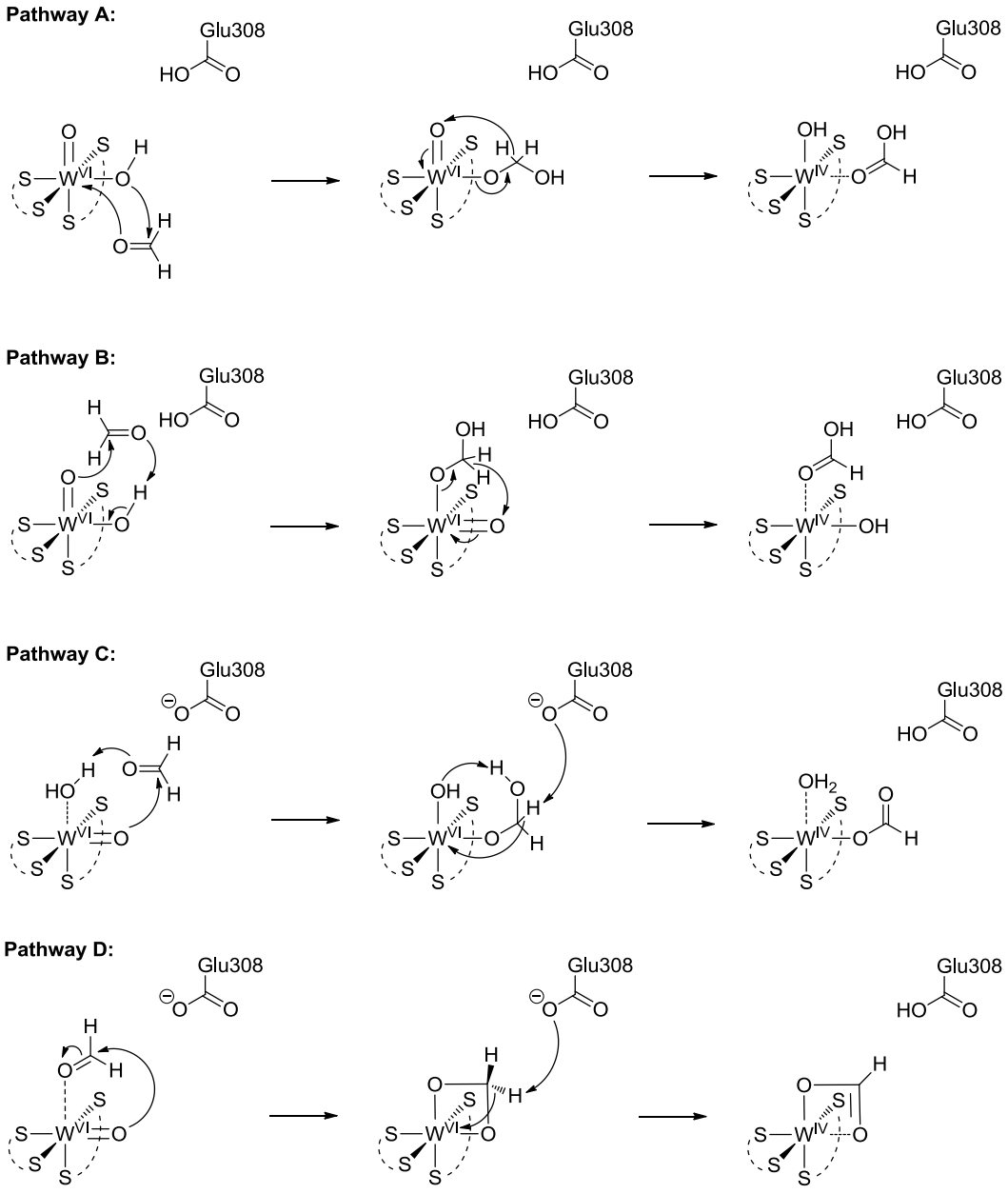

Scheme 6.1. *Four possible pathways investigated for W-FOR.*

For pathway **A**, the tungsten-bound hydroxide performs a nucleophilic attack on the substrate carbonyl carbon to form a tetrahedral intermediate (**A-TS1**). The barrier for this step is calculated to be 34.2 kcal/mol in singlet state. The reason for the high barrier is that at **A-TS1**, the tungsten becomes hepta-coordinated in order to switch the ligands (**Figure 6.1**). The following hydride transfer step (**A-TS2**) also has a very high barrier (32.6 kcal/mol in singlet state). The reason for the high barrier may be that the W-oxo here is a poor hydride acceptor. In Mo-AOR, a Mo-sufido is used to accept the hydride. QM/MM calculations show that the barrier of hydride transfer to sufido is about 15 kcal/mol lower than that to Mo-oxo.[202]

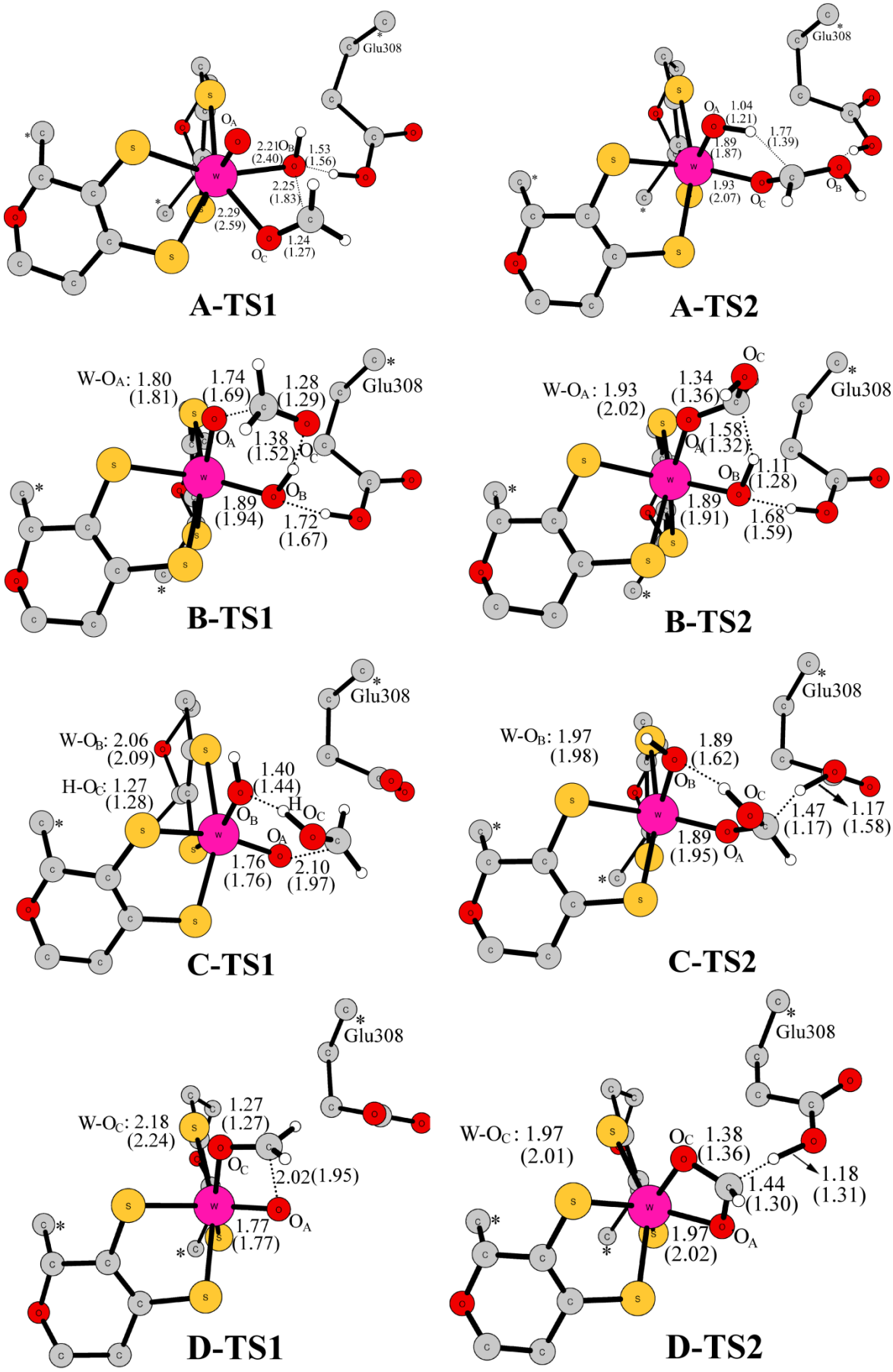

Figure 6.1. *Optimized structures of transition states for pathway **A**, **B**, **C**, and **D**.*

For pathway **B**, W^{VI}=O acts as the nucleophile and the tungsten-bound hydroxide (O_BH^-) protonates the formaldehyde oxygen (**B-TS1**). The barrier now is calculated to be 14.1 kcal/mol for singlet state. The W^{VI}=O is apparently a better nucleophile than the W-OH. Another important feature is that in this mechanism the tungsten avoids becoming hept-coordinated as in **A-TS1**. Similarly to **A-TS2**, the subsequent hydride transfer step (**B-TS2**) also has a quite high barrier (30.8 kcal/mol for singlet state). The high barrier here rules out this mechanistic possibility.

For pathway **C**, the intermediate oxidation proceeds through an alternative mechanistic scenario, in which a base takes a proton and the two-electron transfers to the metal center. In this case, the proton transfer and the two-electron transfer are in opposite direction, rather than in the same direction as in the hydride transfer as shown in pathway **A** and **B**. Glu308 is the most likely candidate of the crucial base. In order to keep Glu308 ionized, both the O_BH^- proton and the neutral Glu308 proton have to transfer to O_A. Similarly to **B-TS1**, W^{VI}=O performs the nucleophilic attack and the water molecule protonates the formaldehyde substrate in **C-TS1**. The barrier for this step is calculated to be 26.1 kcal/mol for singlet. In the following step (**C-TS2**), the proton transfers from the diol carbon to Glu308, coupled with two-electron reduction of W^{VI}. However, the barrier is still as high as 38.7 kcal/mol. This pathway is thus not a viable option.

For pathway **D**, the water molecule is removed from the model and now the formaldehyde carbonyl oxygen is coordinated to W. Then the W^{VI}=O makes a nucleophilic attack on the formaldehyde (**D-TS1**). The barrier is calculated to be 14.3 kcal/mol in singlet state. During the nucleophilic attack, the tungsten ion stabilizes the developed negative charge on formaldehyde O_C, thereby lowering the barrier. The following proton transfer step (**D-TS2**) is also calculated to have quite feasible barrier (14.5 kcal/mol for singlet state). In this mechanism, two electrons transfer to W(VI), resulting in its reduction to W(IV). Thus, pathway D is energetically very feasible.

6.2 Acetylene hydratase (Paper IX)

AH is a tungstoenzyme that catalyzes a non-redox hydration of acetylene during the anaerobic unsaturated hydrocarbon metabolism (**Scheme 6.2**).[203] This reaction is exothermic by 112 kJ/mol, offering thus a significant source of energy for bacteria.[204,205]

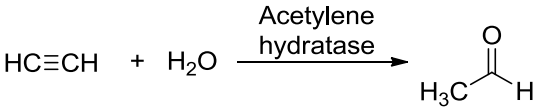

Scheme 6.2. *Reaction catalyzed by acetylene hydratase.*

The crystal structure of AH from *P. acetylenicus* has been solved and it reveals a mononuclear tungsten center in the active site.[203] The tungsten ion is ligated by four sulfur atoms of the two pterin dithiolene moieties, Cys141, and an oxygen species, which was assigned to be a water molecule. Asp13, a second-shell residue, forms a hydrogen bond to the water molecule. Asp13 has been assigned to be protonated based on empirical pH titration calculation.[203] However, an ionized form could also be possible since crystal structure shows that it has two additional hydrogen bonds to the peptide of Cys12-Asp13 and the side chain of Trp179. An arginine residue (Arg606) is located close to the two pterin molecules, providing electrostatic stabilizations to the cofactors.

The reaction mechanism of AH is presently poorly understood. All possible mechanistic proposals can be divided into two groups, first-shell and second-shell mechanisms. Based on the crystal structure, Seiffert et al. proposed a second-shell mechanism in which the W-bound water functions as an electrophile to deliver a proton to the acetylene substrate.[203] Antony and Bayse show that the displacement of water by acetylene is exothermic by more than 20 kcal/mol using density functional calculations together with a small model consisting of the tungsten and its first-shell ligands.[206] Then they suggested that the water molecule performs a nucleophilic attack on the W-bound acetylene, assisted by the neutral Asp13 residue. Most recently, Vincent et al. showed that these two mechanisms have barriers more than 40 kcal/mol, suggesting that these two proposals are not viable.[207] In addition, they speculated that the reaction proceeds through a $W{=}C{=}CH_2$ vinylidene intermediate. However, the barriers for both its formation and also the following steps were shown to be prohibitively high (28.1 and 34.0 kcal/mol, respectively).

From calculations, we found that the mechanism shown in **Scheme 6.3** is energetically most feasible. In this mechanism, the acetylene substrate displaces the W-bound water molecule to form a W-acetylene adduct (**Inter1**). This step is calculated to be exothermic by 5.4 kcal/mol. From **Inter1**, the ionized Asp13 residue activates the water molecule to perform a nucleophilic attack on the acetylene carbon (**TS1**, **Figure 6.2**), affording a vinyl anion intermediate. The barrier for this step is calculated to be 15.9 kcal/mol relative to **Inter1**. Then, Asp13, which becomes neutral in the previous step, delivers a proton to the

intermediate (**TS2**), creating a vinyl alcohol intermediate. This step is calculated to be rate-limiting, associated with a barrier of 23.0 kcal/mol relative to **Inter1** (**Figure 6.3**). The tungsten ion functions as an electrophilic catalyst to stabilize the negative charge in the transition states and the intermediate, thereby lowering the barrier.

Then, an isomerization is needed to generate the final acetaldehyde product. Asp13 shuttles a proton from the hydroxyl group to the C2 of vinyl alcohol (**TS3**). First, a proton transfers from the hydroxyl group to Asp13 (**TS3**), coupled with enolate oxygen coordination to W. Then Asp13 delivers the proton to C2. The second proton transfer step is rate-limiting, with a barrier of 14.1 kcal/mol relative to **Inter4**. The whole reaction is exothermic by 18.4 kcal/mol.

The energies for all stationary points along this pathway are summarized in **Figure 6.3**. It can be seen that **TS2** is rate-limiting, with a barrier of 23.0 kcal/mol.

We have considered other mechanistic possibilities involving a neutral Asp13 residue, but all of them were shown to have high barriers.

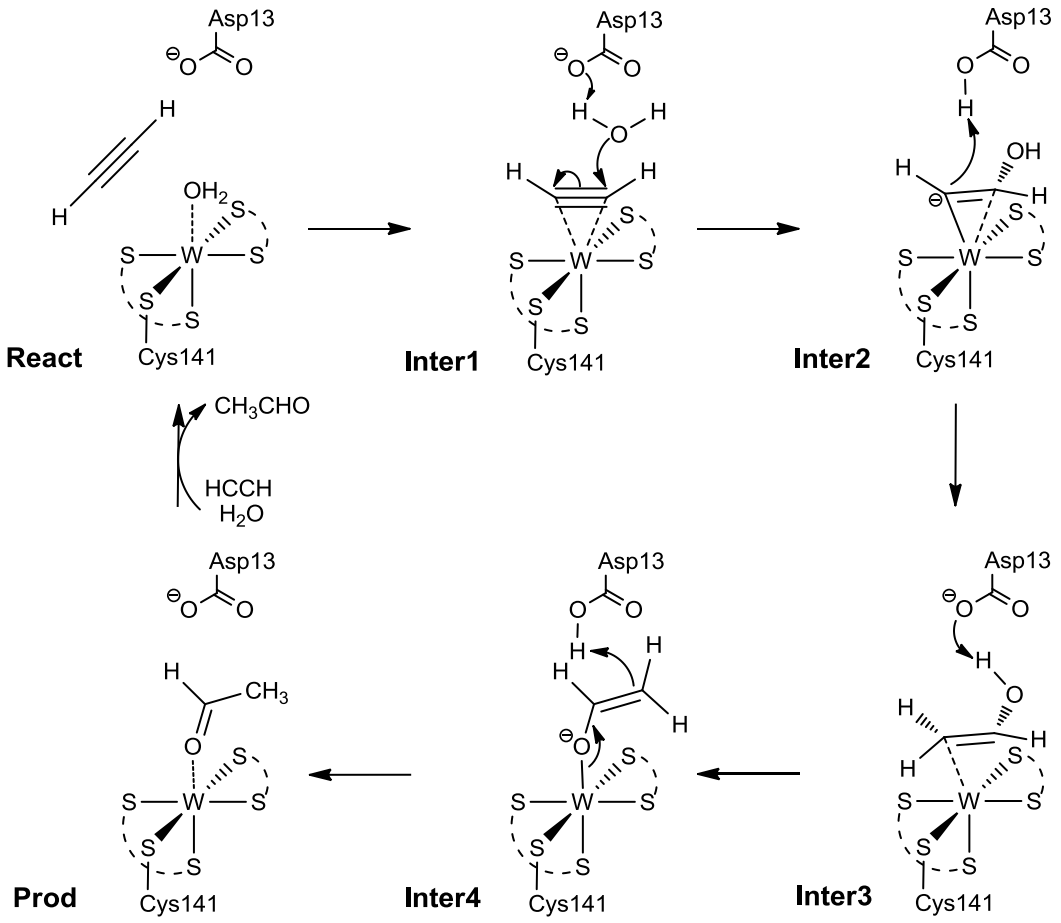

Scheme 6.3*. Suggested acetylene hydration mechanism from calculations.*

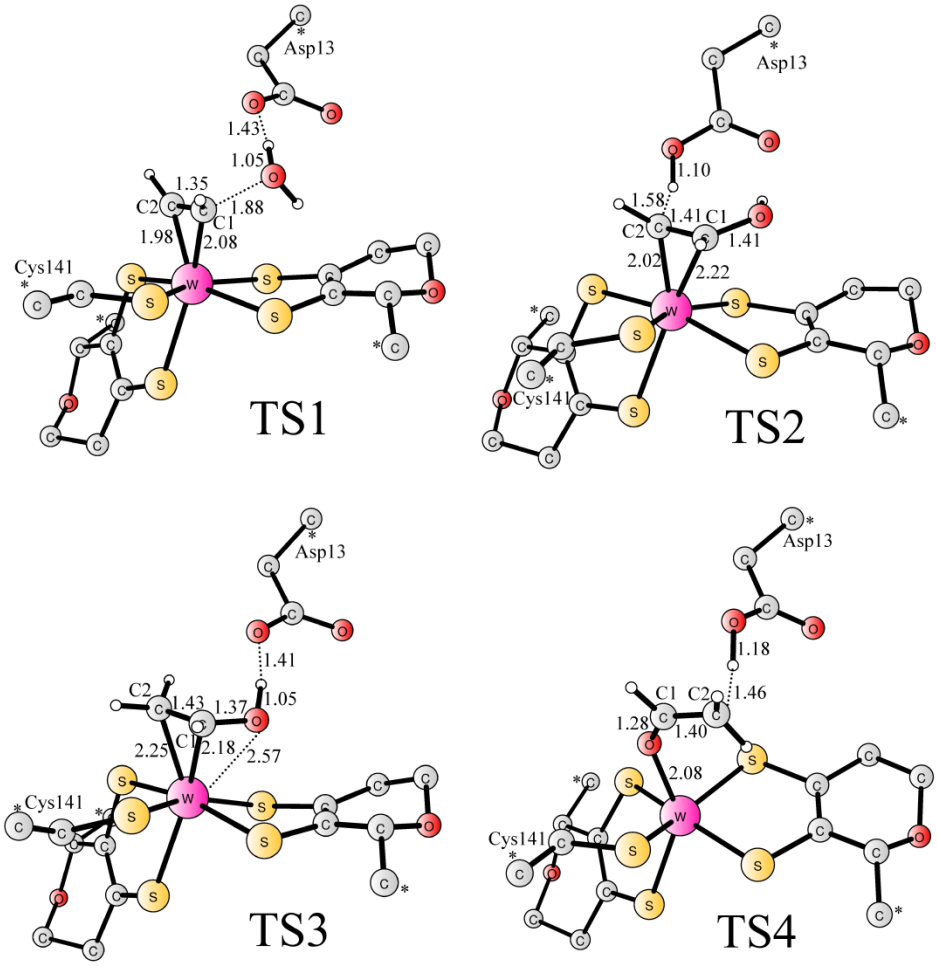

***Figure 6.2**. Optimized structures of transition states for acetylene hydration by AH.*

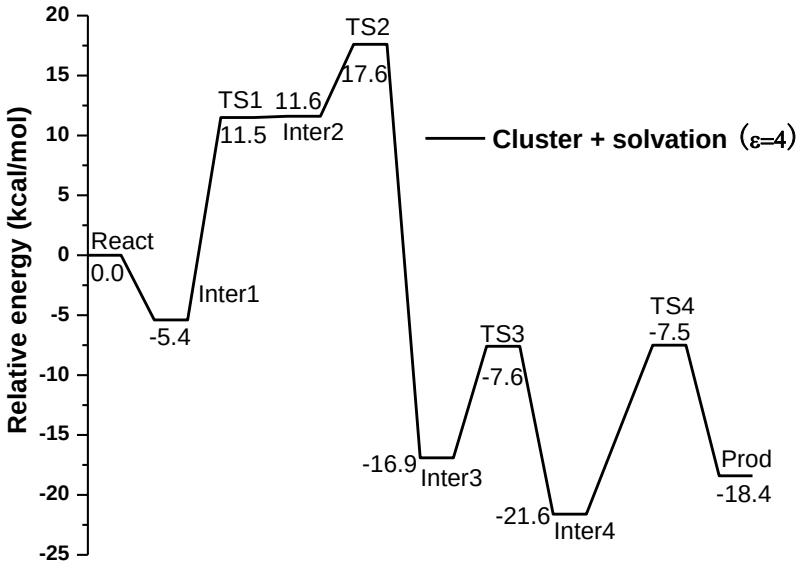

***Figure 6.3**. Calculated potential energy profile for acetylene hydration by AH.*

Chapter 7

Mycolic acid cyclopropane synthase (paper X)

Mycobacterium tuberculosis mycolic acid cyclopropane synthases (MACS) catalyze the cyclopropanation of the double bond of unsaturated mycolic acids, with an S-adenosyl-L-methionine cofactor functioning as the methylene donor.[208-212] A base is needed to take a proton from the methyl group after its transfer. Based on crystal structures of MACS and mutational studies of related *E. coli* cyclopropane fatty acid synthase (CFAS), a bicarbonate ion has been suggested to function as the base.[213-215] In addition, Se-adenosylmethionine and Te-adenosylmethionine substitution experiments suggested that the first step is rate-limiting.[216]

Here, we give support to the experimental proposal for the reaction mechanism and provide details about the reaction pathway and the associated energetics. First, the non-enzymatic reaction is studied in order to compare with the enzymatic reaction, which will be helpful in the analysis of the effect of the various parts in the enzyme active site. A truncated sulfanium cation is used to mimic the SAM cofactor and a 3-hexene molecule as a model substrate. The methyl transfer is calculated to take place through an S_N2 mechanism (**Figure 7.1**), associated with a barrier of 29.2 kcal/mol with ε=80. The resulting carbocation intermediate lies at +20.1 kcal/mol (ε=80). In the intermediate, the methyl group is asymmetrically bound to the double bond. The enzyme environment has to lower the barrier for the methyl transfer by ca 10 kcal/mol (experimental barrier: 19 kcal/mol). In addition, a suitable base is needed to abstract the proton from the intermediate to complete the reaction.

For the enzymatic reaction, a large model of the active site with about 180 atoms is designed. The important Glu140 residue, being hydrogen-bonded to the base bicarbonate, is modeled in both the ionized and the neutral forms.

When Glu140 is ionized, the barrier for the first methyl transfer step is calculated to be 23.9 kcal/mol, which is thus about 5 kcal/mol lower than that of no-enzymatic model. At **TS1** (**Figure 7.2**), the S-C distance is slightly longer than the corresponding distance in methyltransferases with nitrogen as an acceptor.[217-219] The Gly137-Ala138 and Tyr33-Ser34 peptide oxygens interact with the transferred methyl group, providing stabilization to the

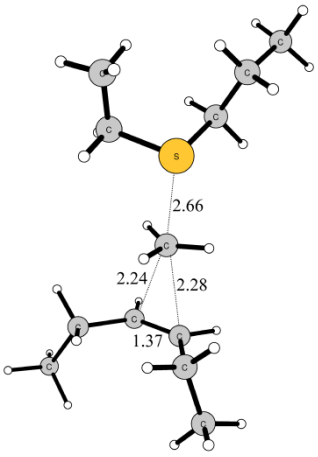

***Figure 7.1**. Optimized structure of transition state for the non-enzymatic reaction.*

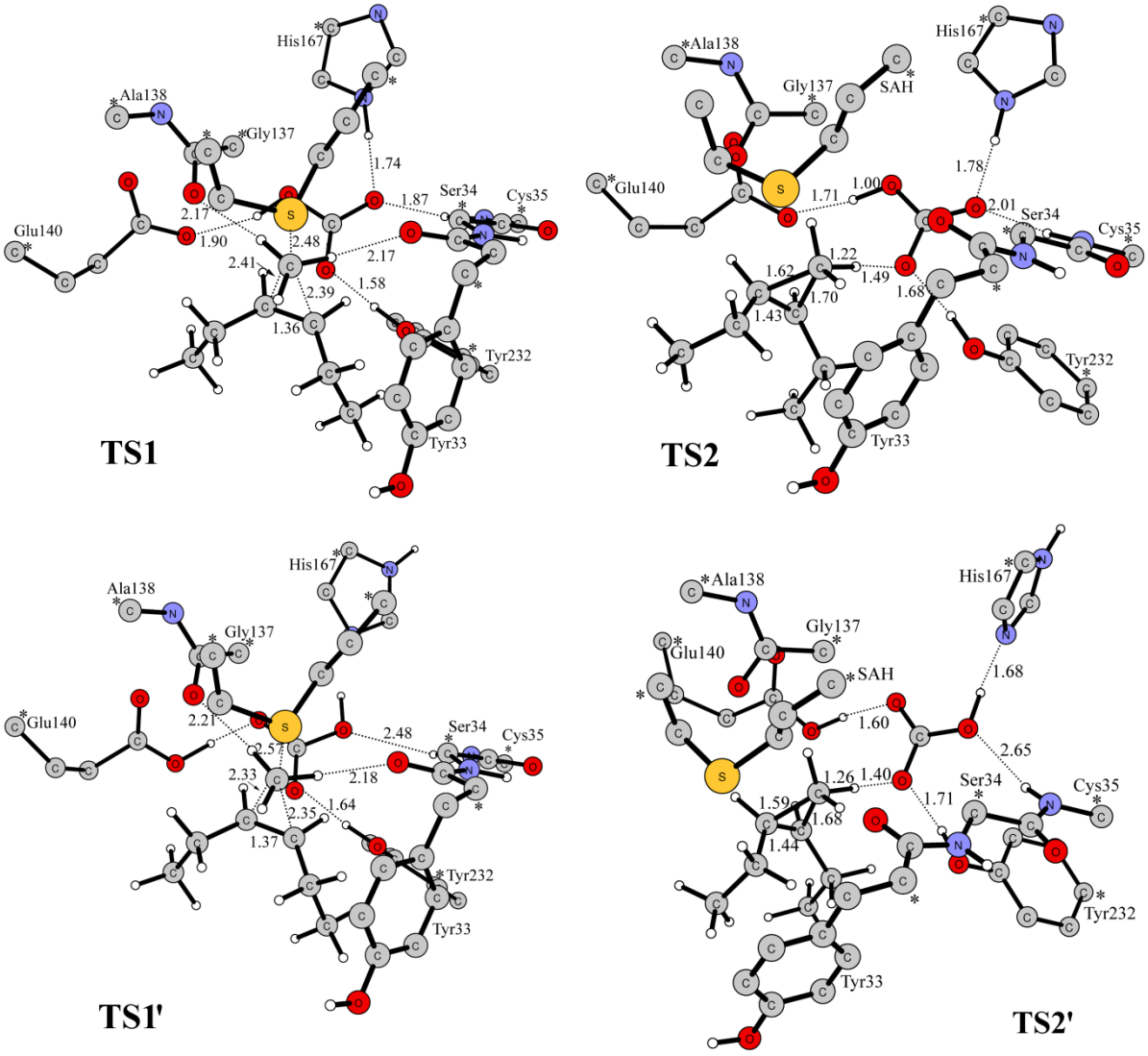

***Figure 7.2**. Optimized structures of transition state for the enzymatic reaction with ionized Glu140 (up) and neutral Glu140 (down).*

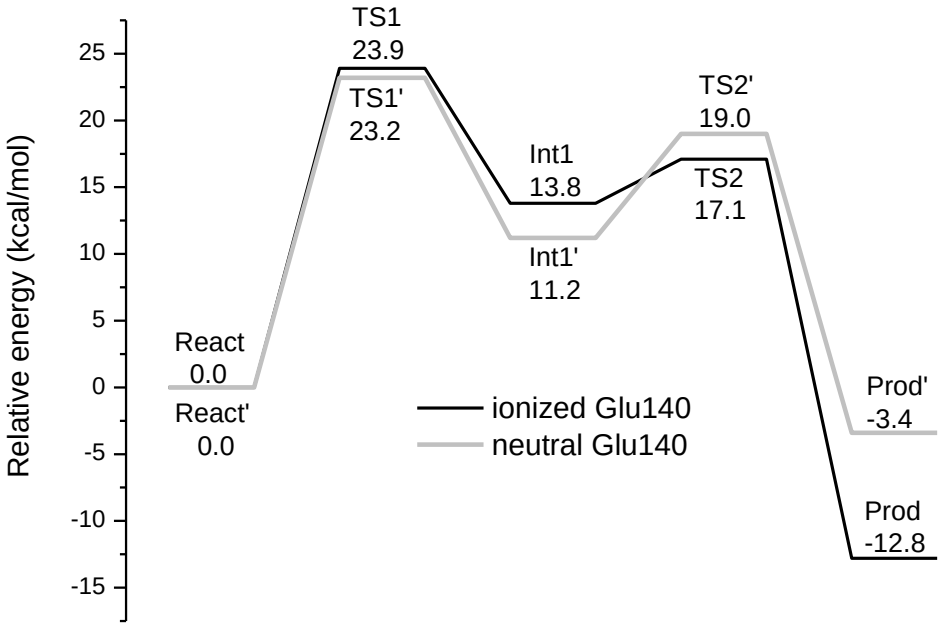

Figure 7.3*. Calculated potential energy profiles for the enzymatic reaction with ionized Glu140 and neutral Glu140.*

methyl carbocation in **TS1**, lowering thus the barrier. The bicarbonate also provides electrostatic stabilization to the resulting carbocation intermediate. In the second step, three events are seen to take place concertedly, namely a proton transfer from the methyl group of the carbocation to the bicarbonate, a proton transfer from bicarbonate to Glu140, and ring closure to form the cyclopropane product. In this case, the bicarbonate functions as a bridge to shuttle the proton from the carbocation to Glu140. The barrier is calculated to be only 3.3 kcal/mol from the intermediate (**Figure 7.3**). Thus the first step is rate-limiting, in accordance with the onium chalcogen effect experiments. Experimental rate constants were measured to be in the range of 2-12 min^{-1}, which can be converted to barriers around 19 kcal/mol using classical transition state theory. The calculated barrier of 23.9 kcal/mol is thus in quite good agreement, but somewhat overestimated. Similar behavior was also seen in the previous study on the mechanism of methylguanine-DNA methyltransferase.[220]

When Glu140 is neutral, the barrier for the first methyl transfer step (**TS1'**, **Figure 7.2**) is 23.2 kcal/mol, very similar to that with ionized Glu140. However, for the second step, now Glu140 is neutral, the bicarbonate acts as a base to take a proton from the methyl group, concomitantly with the ring closure. The barrier now becomes 19.0 kcal/mol relative to its reactant complex.

The sulfur ylide mechanism that has already been ruled out is also examined to compare the energies. In organic synthesis, a strong base is used to generate the reactive sulfur ylide.[221-225] In the active site of MACS, a possible base could be the bicarbonate, even though it does not directly interact with the methyl group. However, bicarbonate is not expected to be strong enough to accomplish this. We have optimized the ylide intermediate structure with one proton transferred from the methyl group to the bicarbonate ion for both models with ionized and neutral Glu140. Indeed, the energy of the ylide intermediate for both cases is more than 35 kcal/mol higher than its corresponding reactant complex. Thus, here we further confirm that a sulfur ylide mechanism is not energetically viable.

Chapter 8

Concluding remarks

In this thesis, the quantum chemical cluster approach has been used to model enzyme active sites and reaction mechanisms. Six multinuclear zinc enzymes, two tungstoenzymes and a cyclopropane synthase have been investigated.

By modeling of the active site of aspartate decarboxylase with various sizes, it is demonstrated that the solvation effects diminish at a size of ca 150-200 atoms and the choice of the dielectric constant turns out to be rather insignificant.

For all six zinc enzymes, the calculations have established that the bridging hydroxide performs the nucleophilic attack directly from the bridging position. The monozinc bound water attack mechanism in PLC was shown to be energetically less favorable. For enzymes with carbonyl substrates, like DHO, AHL lactonase, and hrDP, the zinc ion with less negatively-charged ligands provide electrostatic stabilization on the oxygen anion during the nucleophilic attack. For enzymes with phosphate substrates, like RNase Z, PLC, and NP1, all zinc ions stabilize the penta-coordinated transition states in the reaction. All substrates for these enzymes have poor leaving groups, and a protonation or direct coordination to zinc ion is required for the reaction. In DHO and hrDP, a carboxylate residue shuttles a proton from the bridging hydroxide to the leaving group. In AHL lactonase and NP1, one zinc ion stabilizes the leaving oxyanion. In RNase Z, a Glu-His diad protonates the leaving group. In PLC, a Zn-bound water molecule delivers a proton to the leaving group.

For the two tungstoenzymes, several possible mechanistic scenarios have been considered and new mechanisms have been suggested based on calculations. In FOR, a W^{6+}=O species is shown to perform a nucleophilic attack on the formaldehyde substrate to form a tetrahedral intermediate, followed by proton transfer and two-electron reduction of W^{6+}. In AH, the tungsten ion activates the acetylene substrate through direct coordination to undergo a nucleophilic attack by a water molecule, assisted by an ionic carboxylate residue. This is then followed by protonation of the leading intermediate from the previous step. A subsequent isomerization to acetaldehyde completes the whole reaction.

For MACS, the calculations reveal a two-step mechanism: an S_N2 methyl transfer from the cofactor SAM to the substrate double bond, followed by proton transfer from the methyl group to bicarbonate. The ylide mechanism has been shown to energetically very unfavorable.

We show that quantum chemical cluster models are able to distinguish between different mechanisms (PLC and FOR), protonation states of important residues (DHO, hrDP, AH, and MACS), and between different substrate binding modes (AHL lactonase) from accurate energies of chemical steps obtained with DFT methods.

Finally, the results in this thesis support that density functional theory, in particular B3LYP, together with cluster models of the enzyme active sites is able to answer mechanistic questions concerned with enzymes. Even through the cluster models contain only a small part of the enzymes, they represent the enzymatic properties quite well, and the catalytic reactions can be well described. Quantum chemical methods are thus a routine tool beside experimental techniques to the study of enzymatic reactions.

Acknowledgments

I have had a wonderful time during my PhD studies at Stockholm, first at Department of Theoretical Chemistry, Royal Institute of technology, and then at Department of Organic Chemistry, Stockholm University. Many people contributed directly or indirectly to make my thesis possible. Here I wish to thank:

Prof. Fahmi Himo, my supervisor, who gave me the opportunity to study in Sweden just after some discussion about enzyme modeling and always advises me of the philosophy how to do good science.

Prof. Jan-Erling Bäckvall, for showing interest in my research.

Prof. Ruo-Zhuang Liu and Prof. Jian-Guo Yu in Beijing Normal University, who introduced me to theoretical chemistry.

Prof. Frank M. Raushel in Texas A&M University, for the collaboration in the study of Dihydroorotase.

All teachers, especially Prof. Yi Luo, Prof. Hans Ågren, Prof. Per Siegbahn, Prof. Margareta Blomberg, Prof. Faris Gel'mukhanov, Prof. Aatto Laaksonen, and Prof. Sason Shaik.

All colleagues, especially Shilv, Kathrin, Polina, Peter, Robin, Tommaso, Martin, Mikael, Stefano, Maria, Oscar, and Lynn.

All friends, who have supported me during my studies in Sweden.

References

1. Szabo, A.; Ostlund, N.S. *Modern Quantum Chemistry*; Dover Publication: New York, **1989**.
2. Cramer, C. J. *Essentials of Computational Chemistry*; John Wiley & Sons Ltd.: New York, **2002**.
3. Lewars, E. *Computational Chemistry*; Kluwer Academic Publishers: New York, **2004**.
4. Piela, L. *Ideas of Quantum Chemistry*; Elsevier B. V.: Oxford, **2007**.
5. Jensen, F. *Introduction to Computational Chemistry*; John Wiley & Sons Ltd.: New York, **2007**.
6. Parr, R. G.; Yang, W. *Density-Functional Theory of Atoms and Molecules*; Oxford University Press: New York, **1989**.
7. Koch, W.; Holthausen, M.C. *A Chemist's Guide to Density Functional Theory;* John Wiley & Sons Ltd.: Weiheim, **2000**.
8. Hohenberg, P.; Kohn, W. *Phys. Rev.* **1964**, 136, B864.
9. Kohn, W.; Sham, L. J. *Phys. Rev.* **1965**, 140, A1133.
10. Dirac, P. A. M. *Proc. Cambridge Philos. Soc.* **1930**, 26, 376.
11. Slater, J. C. *Phys. Rev.* **1951**, 81, 385.
12. Vosko, S. H.; Wilk, L.; Nusair, M. *Can. J. Phys.* **1980**, 58, 1200.
13. Becke, A. D. *J. Chem. Phys.* **1986**, 84, 4524.
14. Becke, A. D. *J. Chem. Phys.* **1988**, 88, 1503.
15. Perdew, J. P.; Burke, K.; Ernzerhof, M. *Phys. Rev. Lett.* **1996**, 77, 3865.
16. Lee, C.; Yang, W.; Parr, R. G. *Phys. Rev. B* **1988**, 37, 785.
17. Becke, A. D. *J. Chem. Phys.* **1996**, 104, 1040.
18. Tao, J.; Perdew, J. P.; Staroverov, V. N.; Scuseria, G. E. *Phys. Rev. Lett.* **2003**, 91, 146401.
19. Becke, A. D. *J. Chem. Phys.* **1993**, 98, 1372.
20. Becke, A. D. *J. Chem. Phys.* **1993**, 98, 5648.
21. Bauschlicher, Jr., C.W. *Chem. Phys. Lett.* **1995**, 246, 40.
22. Sousa, S. F.; Fernandes, P. A.; Ramos, M. J. *J. Phys. Chem. B* **2007**, 111, 9146.
23. Sousa, S. F.; Carvalho, E. S.; Ferreira, D. M.; Tavares, I. S.; Fernandes, P. A.; Ramos, M. J.; Gomes, J. A. N. F. *J. Comput. Chem.* **2009**, 30, 2752.
24. Rayón, V. M.; Valdés, H.; Díaz, N.; Suárez, D. *J. Chem. Theory Comput.* **2008**, 4, 243.
25. Amin, E. A.; Truhlar, D. G. *J. Chem. Theory Comput.* **2008**, 4, 75.
26. Sorkin, A.; Truhlar, D. G.; Amin, E. A. *J. Chem. Theory Comput.* **2009**, 5, 1254.
27. Curtiss, L. A.; Redfern, P. C.; Raghavachari, K. *J. Chem. Phys.* **2005**, 123, 124107.
28. Tirado-Rives, J.; Jorgensen, W. L. *J. Chem. Theory Comput.* **2007**, 4, 297.
29. Riley, K. E.; Merz, K. M. Jr. *J. Phys. Chem. A* **2007**, 111, 6044.
30. Siegbahn, P. E. M. *J. Biol. Inorg. Chem.* **2006,** 11, 695.
31. Mori-Sánchez, P.; Cohen, A. J.; Yang, W.-T. *J. Chem. Phys.* **2006**, 125, 201102.
32. Mori-Sánchez, P.; Cohen, A. J.; Yang, W.-T. *Phys. Rev. Lett.* **2008**, 100, 146401.

33. Cohen, A. J.; Mori-Sánchez, P.; Yang, W.-T. *Science* **2008**, 321, 792.
34. Cohen, A. J.; Mori-Sánchez, P.; Yang, W.-T. *J. Chem. Phys.* **2008**, 129, 121104.
35. Zhao, Y. ; Truhlar, D. G. *Acc. Chem. Res.* **2008**, 41, 157.
36. Blomberg, L. M.; Blomberg, M. R. A.; Siegbahn, P. E. M. *J. Inorg. Biochem.* **2005**, 99, 949.
37. Bassan, A.; Borowski, T.; Siegbahn, P. E. M. *J. Chem. Soc. Dalton Trans.* **2004**, 3153.
38. Grimme, S. *J. Comput. Chem.* **2004**, 25, 1463.
39. Siegbahn, P. E. M.; Blomberg, M. R. A. *Annu. Rev. Phys. Chem.* **1999**, 50, 221.
40. Siegbahn, P. E. M.; Blomberg, M. R. A. *Chem. Rev.* **2000**, 100, 421.
41. Blomberg, M. R. A.; Siegbahn, P. E. M. *J. Phys. Chem. B* **2001**, 105, 9375.
42. Siegbahn, P. E. M. *J. Comput. Chem.* **2001**, 22, 1634.
43. Siegbahn, P. E. M. *Curr. Opin. Chem. Biol.* **2002**, 6, 227.
44. Himo, F.; Siegbahn, P. E. M. *Chem. Rev.* **2003**, 103, 2421.
45. Noodleman, L.; Lovell, T.; Han, W-G.; Li, J.; Himo, F. *Chem. Rev.* **2004**, 104, 459.
46. Siegbahn, P. E. M.; Borowski, T. *Acc. Chem. Res.* **2006**, 39, 729.
47. Himo, F. *Theo. Chem. Acc.* **2006**, 116, 232.
48. Ramos, M. J.; Fernandes, P. A. *Acc. Chem. Res.* **2008**, 41, 689.
49. Himo, F.; Siegbahn, P. E. M. *J. Biol. Inorg. Chem.* **2009**, 14, 643.
50. Blomberg, M. R. A.; Siegbahn, P. E. M. *Biochim. Biophys. Acta* **2010**, 1797, 129.
51. Siegbahn, P. E. M.; Blomberg, M. R. A. *Chem. Rev.* **2010**, 110, online. http://pubs.acs.org/doi/abs/10.1021/cr100070p.
52. Radzicka, A.; Wolfenden, R. *Science* **1995**, 267, 90.
53. Fischer, E. *Ber. Dtsch. Chem. Ges.* **1894**, 27, 3189.
54. Haldane, J. B. S. *Enzymes*; Longmans, Green, London, **1930**.
55. Pauling, L. *Nature* **1948**, 161, 707.
56. Warshel, A.; Sharma, P. K.; Kato, M.; Xiang, Y.; Liu, H.; Olsson, M. H. M. *Chem Rev.* **2006**, 106, 3210.
57. Warshel, A. *J. Bio. Chem.* **1998**, 273, 27035.
58. Cannon, W. R.; Singleton, S. F.; Benkovic, S. J. *Nat. Struc. Biol.* **1996**, 3, 821.
59. Khanjin, N. A.; Snyder, J. P.; Menger, F. M. *J. Am. Chem. Soc.* **1999**, 121, 11831.
60. Wu, N.; Mo, Y.; Gao, J.; Pai, E. P. *Proc. Natl. Acad. Sci. U.S.A.* **2000**, 97, 2017.
61. Jensen, K. P.; Ryde, U. *J. Am. Chem. Soc.* **2005**, 127, 9117.
62. Anderson, V. E. *Arch. Biochem. Biophys.* **2005**, 433, 27.
63. Giraldo, J.; Roche, D.; Rovira, X.; Serra, J. *FEBS Lett.* **2006**, 580, 2170.
64. Karplus, M.; McCammon, J. A. *Annu. Rev. Biochem.* **1983**, 53, 263.
65. Sutcliffe, M. J.; Scrutton, N. S. *Trends Biochem. Sci.* **2000**, 25, 405.
66. Antoniou, D.; Basner, J.; Núñez, S.; Schwartz, S. D. *Chem Rev.* **2006**, 106, 3170.
67. Bruice, T. C.; Benkovic, S. J. *Biochemistry* **2000**, 39, 6267.
68. Bruice, T. C. *Acc. Chem. Res.* **2002**, 35, 139.

69. Hur, S.; Bruice, T. C. *J. Am. Chem. Soc.* **2003**, 125, 1472.
70. Kollman, P. A.; Kuhn, B.; Donini, O.; Perakyla, M.; Stanton, R.; Bakowies, D. *Acc. Chem. Res.* **2001**, 34, 72.
71. Devi-Kesavan, L. S.; Gao, J. *J. Am. Chem. Soc.* **2003**, 125, 1532.
72. Cleland, W. W.; Kreevoy, M. M. *Science* **1994**, 264, 1887.
73. Zhang, X. Y.; Houk, K. N. *Acc. Chem. Res.* **2005**, 38, 379.
74. Warshel, A.; Levitt, M. *J. Mol. Biol.* **1976**, 103, 227.
75. Field, M. J.; Bash, P. A.; Karplus, M. *J. Comput. Chem.* **1990**, 11, 700.
76. Gao, J. *Acc. Chem. Res.* **1996**, 29, 298.
77. Monard, G.; Merz, K. M. Jr. *Acc. Chem. Res.* **1999**, 32, 904.
78. Gao, J. L.; Truhlar, D. G. *Annu. Rev. Phys. Chem.* **2002**, 53, 467.
79. Martí, S.; Roca, M.; Andrés, J.; Moliner, V.; Silla, E.; Tuñón, I.; Bertrán, J. *Chem. Soc. Rev.* **2004**, 33, 98.
80. Friesner, R. A.; Guallar, V. *Annu. Rev. Phys. Chem.* **2005**, 56, 389.
81. Senn, H. M.; Thiel, W. *Curr. Opin. Chem. Biol.* **2007**, 11, 182.
82. Senn, H. M.; Thiel, W. *Top. Curr. Chem.* **2007**, 268, 173.
83. Hu, H.; Yang, W. *Annu. Rev. Phys. Chem.* **2008**, 59, 573.
84. Senn, H. M.; Thiel, W. *Angew. Chem. Int. Ed.* **2009**, 48, 1198.
85. Lonsdale, R.; Ranaghan, K. E.; Mulholland, A. J. *Chem. Comm.* **2010**, 46, 2354.
86. Mulholland, A. J.; Grant, G. H.; Richards, W. G. *Protein Eng.* **1993**, 6, 133.
87. Sevastik, R.; Himo, F. *Bioorg. Chem.* **2007**, 35, 444.
88. Hopmann, K. H.; Himo, F. *J. Chem. Theor. Comp.* **2008**, 4, 1129.
89. Georgieva, P. Himo, F. *J. Comput. Chem.* **2010**, 31, 1707.
90. Liao, R. Z.; Himo, F. *manuscript*.
91. Humphrey, W.; Dalke, A.; Schulten, K. *J. Mol. Graphics* **1996**, 14, 33.
92. www.yasara.org/index.html.
93. Hough, E.; Hansen, L. K.; Birknes, B.; Jynge, K.; Hansen, S.; Hordvik, A.; Little, C.; Dodson, E.; Derewenda, Z. *Nature* **1989**, 338, 357.
94. Kim, M. H.; Choi, W.-C.; Kang, H. O.; Lee, J. S.; Kang, B. S.; Kim, K. J.; Derewenda, Z. S.; Oh, T.-K.; Lee, C H.; Lee, J.-K. *Proc. Natl. Acad. Sci. U.S.A.* **2005**, 102, 17606.
95. Gaussian 03, Revision D.01, Frisch, M. J.; Trucks, G. W.; Schlegel, H. B.; Scuseria, G. E.; Robb, M. A.; Cheeseman, J. R.; Montgomery, Jr., J. A.; Vreven, T.; Kudin, K. N.; Burant, J. C.; Millam, J. M.; Iyengar, S. S.; Tomasi, J.; Barone, V.; Mennucci, B.; Cossi, M.; Scalmani, G.; Rega, N.; Petersson, G. A.; Nakatsuji, H.; Hada, M.; Ehara, M.; Toyota, K.; Fukuda, R.; Hasegawa, J.; Ishida, M.; Nakajima, T.; Honda, Y.; Kitao, O.; Nakai, H.; Klene, M.; Li, X.; Knox, J. E.; Hratchian, H. P.; Cross, J. B.; Bakken, V.; Adamo, C.; Jaramillo, J.; Gomperts, R.; Stratmann, R. E.; Yazyev, O.; Austin, A. J.; Cammi, R.; Pomelli, C.; Ochterski, J. W.; Ayala, P. Y.; Morokuma, K.; Voth, G. A.; Salvador, P.; Dannenberg, J. J.; Zakrzewski, V. G.; Dapprich, S.; Daniels, A. D.; Strain, M. C.;

Farkas, O.; Malick, D. K.; Rabuck, A. D.; Raghavachari, K.; Foresman, J. B.; Ortiz, J. V.; Cui, Q.; Baboul, A. G.; Clifford, S.; Cioslowski, J.; Stefanov, B. B.; Liu, G.; Liashenko, A.; Piskorz, P.; Komaromi, I.; Martin, R. L.; Fox, D. J.; Keith, T.; Al-Laham, M. A.; Peng, C. Y.; Nanayakkara, A.; Challacombe, M.; Gill, P. M. W.; Johnson, B.; Chen, W.; Wong, M. W.; Gonzalez, C.; and Pople, J. A.; Gaussian, Inc., Wallingford CT, **2004**.

96. Hay, P. J.; Wadt, W. R. *J. Chem. Phys.* **1985**, 82, 270.
97. Roy, L. E.; Hay, P. J.; Martin, R. L. *J. Chem. Theory Comput.* **2008**, 4, 1029.
98. Klamt, A.; Schüürmann, G. *J. Chem. Soc., Perkin. Trans.* **1993**, 2, 799.
99. Andzelm, J.; Kölmel, C.; Klamt, A. *J. Chem. Phys.* **1995**, 103, 9312.
100. Barone, V.; Cossi, M. *J. Phys. Chem. A* **1998**, *102*, 1995.
101. Cossi, M.; Gega, N.; Scalmani, G.; Barone, V. *J. Comput. Chem.* **2003**, 24, 669.
102. Hu, P.; Zhang, Y. *J. Am. Chem. Soc.* **2006**, 128, 1272.
103. Peng, C.; Ayala, P. Y.; Schlegel, H. B.; Frisch, M. J. *J. Comput. Chem.* **1996**, 17, 49.
104. Williamson, J. M.; Brown, G. M. *J. Biol. Chem.* **1979**, 254, 8074.
105. Cronan, J. E. Jr *J. Bacteriol.* **1980**, 141, 1291.
106. van Poelje, P. D.; Snell, E. E. *Annu. Rev. Biochem.* **1990**, 59, 29.
107. Ramjee, M. K.; Genschel, U.; Abell, C.; Smith, A. G. *Biochem. J.* **1997**, 323, 661.
108. Chopra, S. C.; Pai, H.; Ranganathan, A. *Protein Expression Purif.* **2002**, 25, 533.
109. Lee, B. I.; Suh, S. W. *J. Mol. Biol.* **2004**, 340, 1.
110. Kirkwood, J. G. *J. Chem. Phys.* **1934**, 2, 351.
111. Onsager, L. *J. Am. Chem. Soc.* **1936**, 58, 1486.
112. Eyring, H. *J. Chem. Phys.* **1935**, 3, 107.
113. Truhlar, D. G.; Garrett, B. C.; Klippenstein, S. J. *J. Phys. Chem.* **1996**, 100, 12771.
114. Holm, L.; Sander, C. *Proteins: Struct. Funct. Genet.* **1997**, 28, 72.
115. Washabaugh, M. W.; Collins, K. D. *J. Biol. Chem.* **1984**, 259, 3293.
116. Christopherson, R. I.; Lyons, S. D. *Med. Res. Rev.* **1990**, 10, 505.
117. Jones, M. E. *Annu. Rev. Biochem.* **1980**, 49, 253.
118. Thoden, J. B.; Phillips, G. N. Jr.; Neal, T. M.; Raushel, F. M.; Holden, H. M. *Biochemistry* **2001**, 40, 6989.
119. Lee, M.; Chan, C. W.; Guss, J. M.; Christopherson, R. I.; Maher, M. J. *J. Mol. Biol.* **2005**, 348, 523.
120. Adachi, H.; Tawaragi, Y.; Inuzuka, C.; Kubota, I.; Tsujimoto, M.; Nishihara, T.; Nakazato, H. *J. Biol. Chem.* **1990**, 265, 3992.
121. White, I. J.; Lawson, J.; Williams, C. H.; Hooper, N. M. *Anal. Biochem.* **1999**, 268, 245.
122. Rajotte, D.; Ruoslahti, E. *J. Biol. Chem.* **1999**, 274, 11593.
123. Kim, H. S.; Canpbell, B. J. *Biochem. Biophys. Res. Commun.* **1982**, 108, 1638.
124. Campbell, B. J.; Forrester, L. J.; Zahler, W.; Burks, M. *J. Biol. Chem.* **1984**, 259, 14586.
125. Kropp, H.; Sundelof, J. G.; Hajdu, R.; Kahan, F. M. *Antimicrob. Agents Chemother.* **1982**, 22, 62.

126. Nitanai, Y.; Satow, Y.; Adachi, H.; Tsujimoto, M. *J. Mol. Biol.* **2002**, 321, 177.
127. Kahan, F. M.; Kropp, H.; Sundelof, J. G.; Birnbaum, J. *J. Antimicrob. Chemother.* **1983**, 12, 1.
128. Buckhaults, P.; Rago, C.; Croix, B. S.; Romans, K. E.; Saha, S.; Zhang, L.; Vogelstein, B.; Kinzler, K. W. *Cancer Res.* **2001**, 61, 6996.
129. Liao, R.-Z.; Yu, J.-G.; Raushel, F. M.; Himo, F. *Chem. Eur. J.* **2008**, 14, 4287.
130. Chen, S.-L.; Marino, T.; Fang, W.-H.; Russo, N.; Himo, F. *J. Phys. Chem. B* **2008**, 112, 2494.
131. Schürer, G.; Lanig, H.; Clark, T. *Biochemistry* **2004**, 43, 5414.
132. Leopoldini, M.; Russo, N.; Toscano, M. *J. Am. Chem. Soc.* **2007**, 129, 7776.
133. Schürer, G.; Horn, A. H. C.; Gedeck, P.; Clark, T. *J. Phys. Chem. B* **2002**, 106, 8815.
134. Welch, M.; Todd, D. E.; Whitehead, N. A.; McGowan, S. J.; Bycroft, B. W.; Salmond, G. P. C. *EMBO J.* **2000**, 19, 631.
135. Zhang, L. H.; Murphy, P. J.; Kerr, A.; Tate, M. E. *Nature* **1993**, 362, 446.
136. Fray, R. G.; Throup J. P.; Daykin, M.; Wallace, A.; Williams, P.; Stewart, G. S.A.B.; Grierson, D. *Nat. Biotech.* **1999**, 17, 1017.
137. Dong, Y. H.; Gusti, A. R.; Zhang, Q.; Xu, J. L.; Zhang, L. H. *Appl. Environ. Microbiol.* **2002**, 68, 1754.
138. Lee, S. J.; Park, S. Y.; Lee, J. J.; Yum, D. Y.; Koo, B. T.; Lee, J. K. *Appl. Environ. Microbiol.* **2002**, 68, 3919.
139. Dong, Y. H.; Xu, J. L.; Li, X. Z. ; Zhang, L. H. *Proc. Natl. Acad. Sci. U.S.A.* **2000**, 97, 3526.
140. Thomas, P. W.; Stone, E. M.; Costello, A. L.; Tierney, D. L.; Fast, W. *Biochemistry* **2005**, 44, 7559.
141. Liu, D. L.; Lepore, B. W.; Petsko, G. A.; Thomas, P. W.; Stone, E. M.; Fast, W.; Ringe, D. *Proc. Natl. Acad. Sci. U.S.A.* **2005**, 102, 11882.
142. Kim, M. H.; Choi, W.-C.; Kang, H. O.; Lee, J. S.; Kang, B. S.; Kim, K. J.; Derewenda, Z. S.; Oh, T.-K.; Lee, C. H.; Lee, J.-K. *Proc. Natl. Acad. Sci. U.S.A.* **2005**, 102, 17606.
143. Liu, D.; Momb, J.; Moulin, A.; Petsko, G. A.; Fast, W.; Ringe, D. *Biochemistry* **2008**, 47, 7706.
144. Momb, J.; Wang, C.; Liu, D.; Thomas, P. W.; Petsko, G. A.; Guo, H.; Ringe, D.; Fast, W. *Biochemistry* **2008**, 47, 7715.
145. Liao, R.-Z.; Himo, F.; Yu, J.-G.; Liu, R.-Z. *J. Inorg. Biochem.* **2010**, 104, 37.
146. Takaku, H.; Minagawa, A.; Takagi, M.; Nashimoto, M. *Nucleic Acids Res.* **2004**, 32, 4429.
147. Vogel, A.; Schilling, O.; Späth, B.; Marchfelder, A. *Biol. Chem.* **2005**, 386, 1253.
148. Redko, Y.; Li de la Sierra-Gallay, I.; Condon, C. *Nat. Rev. Microbiol.* **2007**, 10, 271.
149. Späth, B.; Canino, G.; Marchfelder, A. *Cell. Mol. Life Sci.* **2007**, 64, 2404.
150. Tavtigian, S. V.; Simard, J.; Teng, D. H. F.; Abtin, V.; Baumgard, M.; Beck, A.; Camp, N. J.; Carillo, A. R.; Chen, Y.; Dayananth, P.; Desrochers, M.; Dumont, M.; Farnham, J. M.; Frank, D.; Frye, C.; Ghaffari, S.; Gupte, J. S.; Hu, R.; Iliev, D.; Janecki, T.; Kort, E. N.; Laity, K. E.; Leavitt, A.; Leblanc, G.; McArthur-Morrison, J.; Pederson, A.; Penn, B.; Peterson, K. T.; Reid, J. E.; Richards, S.; Schroeder, M.; Smith, R.; Snyder, S. C.; Swedlund, B.; Swensen, J.; Thomas, A.; Tranchant, M.; Woodland, A.-M.; Labrie, F.; Skolnick, M. H.; Neuhausen, S.; Rommens, J.; Cannon-Albright, L. A. *Nat. Genet.* **2001**, 27, 172.

151. Li de la Sierra-Gallay, I.; Mathy, N.; Pellegrini, O.; Condon, C. *Nat. Struct. Mol. Biol.* **2006**, 13, 376.
152. Li de la Sierra-Gallay, I.; Pellegrini, O.; Condon, C. *Nature* **2005**, 433, 657.
153. Ishii, R.; Minagawa, A.; Takaku, H.; Takagi, M.; Nashimoto, M.; Yokoyama, S. *J. Biol. Chem.* **2005**, 280, 14138.
154. Kostelecky, B.; Pohl, E.; Vogel, A.; Schilling, O.; Meyer-Klaucke, W. *J. Bacteriol.* **2006**, 188, 1607.
155. Ishii, R.; Minagawa, A.; Takaku, H.; Takagi, M.; Nashimoto, M.; Yokoyama, S. *Acta. Cryst. F* **2007**, 63, 637.
156. Zareen, N.; Yan, H.; Hopkinson, A.; Levinger, L. *J. Mol. Biol.* **2005**, 350, 189.
157. Minagawa, A.; Takaku, H.; Ishii, R.; Takagi, M.; Yokoyama, S.; Nashimoto, M. *Nucleic Acids. Res.* **2006**, *34*, 3811.
158. Karkashon, S.; Hopkinson, A.; Levinger, L. *Biochemistry* **2007**, 46, 9380.
159. Elbarbary, R. A.; Takaku, H.; Nashimoto, M. *Biochim. Biophys. Acta* **2008**, 1784, 2079.
160. Liao, R.-Z.; Yu, J.-G.; Himo, F. *Inorg. Chem.* **2009**, 48, 1442.
161. Exton, J. H. *Eur. J. Biochem.* **1997**, 243, 10.
162. Exton, J. H. *J. Biol. Chem.* **1990**, 265, 1.
163. Hergenrother, P. J.; Martin, S. F. *Anal. Biochem.* **1997**, 251, 45.
164. Hergenrother, P. J.; Martin, S. F. *Top. Curr. Chem.* **2001**, 211, 131.
165. Berridge, M. J. *Biochem. J.* **1984**, 220, 345.
166. Titball, R. W. *Microbiol. Rev.* **1993**, 57, 347.
167. Hough, E.; Hansen, L. K.; Birknes, B.; Jynge, K.; Hansen, S.; Hordvik, A.; Little, C.; Dodson, E.; Derewenda, Z. *Nature* **1989**, 338, 357.
168. Hansen, S.; Hough, E.; Svensson, L. A.; Wong, Y.-L.; Martin, S. F. *J. Mol. Biol.* **1993**, *234*, 179.
169. Hansen, S.; Hansen, L. K.; Hough, E. *J. Mol. Biol.* **1993**, 231, 870.
170. Antikainen, N. M.; Monzingo, A. F.; Franklin, C. L. Robertus, J. D.; Martin, S. F. *Arch. Biochem. Biophys.* **2003**, 417, 81.
171. Thrige, D. D.; Buur, J. R. B.; Jorgensen, S. F. *Biopolym.* **1997**, 42, 319.
172. Sundell, S.; Hansen, S.; Hough, E. *Protein Eng.* **1994**, 7, 571.
173. Berry, R. S. *J. Chem. Phys.* **1960**, 32, 933.
174. More O'Ferrall, R. A. *J. Chem. Soc. B* **1970**, 274.
175. Jencks, W. P. *Chem. Rev.* **1985**, 85, 511.
176. Liao, R.-Z.; Himo, F.; Yu, J.-G.; Liu, R.-Z. *Eur. J. Inorg. Chem.* **2009**, 20, 2967.
177. Martin, S. F.; Hergenrother, P. J. *Biochemistry* **1998**, 37, 5755.
178. Martin, S. F.; Hergenrother, P. J. *Biochemistry* **1999**, 38, 4403.
179. Jones, S.; van Heyningen, P.; Berman, H. M.; Thornton, J. M. *J. Mol. Biol.* **1999**, 287, 877.
180. Jones, S.; Daley, D. T.; Luscombe, N. M.; Berman, H. M.; Thornton, J. M. *Nucleic Acids Res.* **2001**, 29, 943.

181. Luscombe, N. M.; Laskowski, R. A.; Thornton, J. M. *Nucleic Acids Res.* **2001**, 29, 2860.
182. Hoffman, M. M.; Khrapov, M. A.; Cox, J. C.; Yao, J.; Tong, L.; Ellington, A. D. *Nucleic Acids Res.* **2004**, 32, 174.
183. Fujimoto, M.; Kuninaka, A.; Yoshino, H. *Agr. Biol. Chem.* **1974**, 38, 785.
184. Fujimoto, M.; Kuninaka, A.; Yoshino, H. *Agr. Biol. Chem.* **1974**, 38, 1555.
185. Fujimoto, M.; Fujiyama, K.; Kuninaka, A.; Yoshino, H. *Agr. Biol. Chem.* **1974**, 38, 2141.
186. Fujimoto, M.; Kuninaka, A.; Yoshino, H. *Agr. Biol. Chem.* **1975**, 39, 1991.
187. Naik, A. K.; Raghavan, S. C. *DNA Repair* **2008**, 7, 1384.
188. Potter, B. V. L.; Conolly, B. A.; Eckstein, F. *Biochemistry* **1983**, 22, 1369.
189. Romier, C.; Dominguez, R.; Lahm, A.; Dahl, O.; Suck, D. *Proteins* **1998**, 32, 414.
190. Liao, R.-Z.; Yu, J.-G.; Himo, F. *J. Phys. Chem. B.* **2010**, 114, 2533.
191. O'Brien, P. J.; Herschlag, D. *Biochemistry* **2001**, 40, 5691.
192. Johnson, M. K.; Rees, D. C.; Adams, M. W. W. *Chem. Rev.* **1996**, 96, 2817.
193. McMaster, J.; Enemark, J. H. *Curr. Opin. Chem. Biol.* **1998**, 2, 201.
194. L'vov, N. P.; Nosikov, A. N.; Antipov, A. N. *Biochemistry (Moscow)* **2002**, 67, 234.
195. Enemark, J. H. Cooney, J. J. A. *Chem. Rev.* **2004**, 104, 1175.
196. Brondino, C. D.; Romão, M. J.; Moura, I. Moura, J. J. *Curr. Opin. Chem. Biol.* **2006**, 10, 109.
197. Sugimoto, H.; Tsukube, H. *Chem. Soc. Rev.* **2008**, 37, 2609.
198. Bevers, L. E.; Hagedoorn, P.-L.; Hagen, W. R. *Coord. Chem. Rev.* **2009**, 253, 269.
199. Romão, M. J. *Dalton Trans.* **2009**, 4053.
200. Roy, R.; Mukund, S.; Schut, G. J.; Dunn, D. M.; Weiss, R.; Adams, M. W. W. *J. Bacteriol.* **1999**, 181, 1171.
201. Hu, Y.; Faham, S.; Roy, R.; Adams, M. W. W.; Rees, D. C. *J. Mol. Biol.* **1999**, 286, 899.
202. Metz, S.; Wang, D.; Thiel, W. *J. Am. Chem. Soc.* **2009**, 131, 4628.
203. Seiffert, G. B.; Ullmann, G. M.; Messerschmidt, A.; Schink, B.; Kroneck, P. M. H.; Einsle, O. *Proc. Natl. Acad. Sci. USA* **2007**, 104, 3073.
204. Schink, B. *Arch. Microbiol.* **1985**, 142, 295.
205. Rosner, B. M.; Schink, B. *J. Bacteriol.* **1995**, 177, 5767.
206. Antony, S.; Bayse, C. A. *Organometallics* **2009**, 28, 4938.
207. Vincent, M. A.; Hillier, I. H.; Periyasamy, G.; Burton, N. A. *Dalton Trans.* **2010**, 39, 3816.
208. Yuan, Y.; Mead, D.; Schroeder, B. G.; Zhu, Y.-Q.; Barry C. E., III *J. Biol. Chem.* **1998**, 273, 21282.
209. Yuan, Y.; Lee, R. E.; Besra, G. S.; Belisle, J. T.; Barry C. E., III *Proc. Natl. Acad. Sci. USA* **1995**, 92, 6630.
210. Glickman, M. S.; Cox, J. S.; Jacobs, W. R. Jr. *Mol. Cell* **2000**, 5, 717.
211. Glickman, M. S.; Cahill, S. M.; Jacobs, W. R. Jr. *J. Biol. Chem.* **2001**, 276, 2228.
212. Glickman, M. S. *J. Biol. Chem.* **2003**, 278, 7844.

213. Huang, C.; Smith, C. V.; Glickman, M. S.; Jacobs, W. R. Jr.; Sacchettini, J. C. *J. Biol. Chem.* **2002**, 277, 11559.
214. Iwig, D. F.; Uchida, A.; Stromberg, J. A.; Booker, S. J. *J. Am. Chem. Soc.* **2005**, 127, 11612.
215. Courtois, F.; Ploux, O. *Biochemistry* **2005**, 44, 13583.
216. Iwig, D. F.; Grippe, A. T.; McIntyre, T. A.; Booker, S. J. *Biochemistry* **2004**, 43, 13510.
217. Velichkova, P.; Himo, F. *J. Phys. Chem. B* **2005**, 109, 8216.
218. Velichkova, P.; Himo, F. *J. Phys. Chem. B* **2006**, 110, 16.
219. Georgieva, P.; Wu, Q.; McLeish, M. J.; Himo, F. *Biochim. Biophys. Acta* **2009**, 1794, 1831.
220. Georgieva, P.; Himo, F. *Chem. Phys. Lett.* **2008**, 463, 214.
221. Solladié-Cavallo, A.; Diep-Vohuule, A.; Isarno, T. *Angew. Chem. Int. Ed.* **1998**, 37, 1689.
222. Ye, S.; Huang, Z.-Z.; Xia, C.-A.; Tang, Y.; Dai, L.-X. *J. Am. Chem. Soc.* **2002**, 124, 2432.
223. Aggarwal, V. K.; Winn, C. L. *Acc. Chem. Res.* **2004**, 37, 611.
224. Gandelman, M.; Naing, K. M.; Rybtchinski, B.; Poverenov, E.; Ben-David, Y.; Ashkenazi, N.; Gauvin, R. M.; Milstein, D. *J. Am. Chem. Soc.* **2005**, 127, 15265.
225. Ma, M.; Peng, L.; Li, C.; Zhang, X.; Wang, J. *J. Am. Chem. Soc.* **2005**, 127, 15016.